The Sec1–Munc18 protein VPS33B forms a uniquely bidirectional complex with VPS16B

Received for publication, January 8, 2023, and in revised form, March 3, 2023 Published, Papers in Press, April 14, 2023,
https://doi.org/10.1016/j.jbc.2023.104718

Richard J. Y. Liu[1], Yusef Al-Molieh[1], Shao Z. Chen[1], Marko Drobac[1], Denisa Urban[1], Chang H. Chen[1], Helen H. Y. Yao[1], Ryan S. Q. Geng[1], Ling Li[2], Fred G. Pluthero[2], Samir Benlekbir[3], John L. Rubinstein[1,3], and Walter H. A. Kahr[1,2,4,5,*]

From the [1]Department of Biochemistry, University of Toronto, Toronto, Ontario, Canada; [2]Cell Biology Program, and [3]Molecular Medicine Program, Research Institute, Hospital for Sick Children, Toronto, Ontario, Canada; [4]Department of Paediatrics, University of Toronto, Toronto, Ontario, Canada; [5]Division of Haematology/Oncology, The Hospital for Sick Children, Toronto, Ontario, Canada

Reviewed by members of the JBC Editorial Board. Edited by Phyllis Hanson

Loss-of-function variants of vacuolar protein sorting proteins VPS33B and VPS16B (VIPAS39) are causative for arthrogryposis, renal dysfunction, and cholestasis syndrome, where early lethality of patients indicates that VPS33B and VPS16B play essential cellular roles. VPS33B is a member of the Sec1–Munc18 protein family and thought to facilitate vesicular fusion *via* interaction with soluble *N*-ethylmaleimide-sensitive factor attachment protein receptor (SNARE) complexes, like its paralog VPS33A in the homotypic fusion and vacuole sorting complex. VPS33B and VPS16B are known to associate, but little is known about the composition, structure, or function of the VPS33B–VPS16B complex. We show here that human VPS33B–VPS16B is a high molecular weight complex, which we expressed in yeast to perform structural, composition, and stability analysis. Circular dichroism data indicate VPS33B–VPS16B has a well-folded α-helical secondary structure, and size-exclusion chromatography–multiangle light scattering revealed a molecular weight of ∼315 kDa. Quantitative immunoblotting indicated a VPS33B:VPS16B ratio of 2:3. Expression of arthrogryposis, renal dysfunction, and cholestasis syndrome–causing VPS33B missense variants showed L30P disrupts complex formation but not S243F or H344D. Truncated VPS16B (amino acids 143 to 316) was sufficient to form a complex with VPS33B. Small-angle X-ray scattering and negative-staining EM revealed a two-lobed shape for VPS33B–VPS16B. Avidin tagging indicated that each lobe contains a VPS33B molecule, and they are oriented in opposite directions. We propose a structure for VPS33B–VPS16B that allows the VPS33B at each end to interact with separate SNARE bundles and/or SNAREpins, plus associated membrane components. These observations reveal the only known potentially bidirectional Sec1–Munc18 protein complex.

The essential cellular functions of mammalian VPS33B and VPS16B (vacuolar protein sorting 33,16 homolog B) initially came to light with the identification of human variants in *VPS33B* and *VIPAS39* (VPS33B interacting protein, apical-basolateral polarity regulator, Spe-39 homolog; VPS16B) causative for arthrogryposis, renal dysfunction, and cholestasis (ARC) syndrome (1, 2). The multisystemic clinical manifestations of this early lethal condition indicate roles for VPS33B and VPS16B in the development and function of the musculoskeletal system, liver, kidneys, heart, brain, skin, and blood platelets (1–5). VPS33B belongs to the Sec1–Munc18 (SM) family of proteins, predicted to interact with soluble *N*-ethylmaleimide-sensitive factor attachment protein receptors (SNAREs), to facilitate intracellular membrane fusion, which implicates VPS33B in processes such as vesicular trafficking. The discovery that VPS33B binds VPS16B suggested these proteins act together to facilitate trafficking and/or other processes required for the formation of secretory vesicles, such as platelet α-granules that are absent in ARC syndrome patients (4, 5). Several other studies (6–12) have indicated that VPS33B and VPS16B play essential roles in many cell types.

Vesicular trafficking in eukaryotic cells involves complex molecular machinery that mediates vesicle budding, movement, docking, and fusion (13). Cells utilize membrane-bound vesicles and other carriers to transport proteins and lipids between cellular compartments. Vesicle fusion with a target membrane is mediated by a conserved apparatus containing SNAREs and SM protein family components. Vesicle-anchored SNAREs associate with target membrane–associated SNAREs to form trans–SNARE complexes between two membrane bilayers that drive membrane fusion (14). However, trans–SNARE complexes do not assemble efficiently unless activated by SM proteins (14), which recent research suggests function as chaperones to enable fast and accurate SNARE assembly (15). In the absence of SM proteins, SNAREs misassemble into nonfunctioning structures (15, 16). Regulation is also achieved through the actions of Rab-GTPases and membrane tethers (15, 17–19). Tethering factors that link transport vesicles to their cognate target membranes can be long coiled-coil proteins or multiunit tethering complexes (20).

The homotypic fusion and vacuole protein sorting (HOPS) and class C core vacuole/endosome tethering (CORVET)

* For correspondence: Walter H. A. Kahr, walter.kahr@sickkids.ca.

complexes of *Saccharomyces cerevisiae* are well-studied membrane tethering complexes that are conserved in eukaryotes from yeast to humans. In yeast, Vps11, Vps16, Vps18, and Vps33 form the class C VPS complex, with core subunits shared by both HOPS and CORVET (21, 22). In this system, Vps33 binds to the syntaxin-like target membrane–associated SNARE Vam3 to facilitate Golgi-to-vacuole and vacuole-to-vacuole fusion events (23). The crystal structure of yeast Vps33p bound to two separate membrane-resident SNAREs suggests that Vps33p may act as a SNARE assembly template (24). The recently determined cryo-EM structure of yeast HOPS revealed an elongated six-member complex with a rigid SNARE-binding core module and flexible extremities where GTPase binding occurs (25).

The composition of complexes containing VPS33B and VPS16B has been debated in the literature. Initial reports suggested that VPS33B and VPS16B may be interchangeable components of the HOPS–CORVET complex (26–28), whereas more recent data suggest that HOPS–CORVET contains only their paralogs VPS33A and VPS16A (25, 29–31). Biochemical studies of VPS33B and VPS16B and the HOPS–CORVET complex components in various cells have further delineated their discrete vesicular trafficking functions (7, 12, 30–35). VPS33B and VPS16B are only found in metazoans (5), where they appear to be essential for several developmental and physiological processes. These include spermatogenesis in *Caenorhabditis elegans* (27), immune defense in *Drosophila* (6, 7), liver development in zebrafish (36), and multiorgan development in humans (1, 2, 4, 5, 10) and mice, where germline homozygous deletion of *Vps33B* is lethal before embryonic day 10.5 (11).

Human variants resulting in loss of VPS33B or VPS16B specifically abrogate α-granule development in platelet precursor megakaryocytes (3–5), whereas in mice, a *VPS33A* variant affects only δ-granule formation (37). This points to distinct cellular functions of these proteins and the complexes they form. Similarly, in *Drosophila*, dVps33A and dVps33B are part of different complexes with nonredundant functions: dVps33A/dVps16A and dVps33B/dVps16B (34).

It has been proposed that dimeric VPS33B–VPS16B bears a structural resemblance to the HOPS–CORVET termed class C homologs in endosome–vesicle interaction tethering complex (38, 39). However, proteomic studies have suggested that dimeric VPS33B–VPS16B is considerably smaller (40), and size-exclusion chromatography (SEC) and immunoblotting have also indicated that the VPS33B–VPS16B complex has a smaller hydrodynamic radius than the HOPS–CORVET complex (41), which is estimated to be 580.7 kDa in humans. The recently determined structure of the yeast HOPS complex reveals an extended and slender structure approximately 430 Å in height and 130 Å in width, with a triangular shape (25).

Here, we show for the first time that human VPS33B and VPS16B form a unique multimeric complex that is structurally distinct from the mammalian HOPS–CORVET complex. To obtain sufficient quantities for detailed biochemical analysis, we established expression of human VPS33B and VPS16B in *S. cerevisiae* and affinity purification methods for isolating VPS33B–VPS16B. We determined that VPS33B–VPS16B exists as a stable complex containing only VPS33B and VPS16B, which when analyzed *via* native gel electrophoresis is comparable to complex expressed in human cells. SEC–multiangle light scattering (SEC–MALS) analysis of VPS33B–VPS16B yielded an estimated molecular weight (MW) of approximately 315 kDa. Quantitative immunoblotting showed this complex consists of two copies of VPS33B associated with three copies of VPS16B. Small-angle X-ray scattering (SAXS), and single particle negative-staining transmission EM revealed that VPS33B and VPS16B form a stable two-lobed structure. Using avidin tagging, we determined that individual copies of VPS33B form the cores of each lobe oriented in trans, a unique bidirectional configuration for SM proteins that may give VPS33B–VPS16B an indispensable role in specific intracellular membrane fusion events.

Results

VPS33B and VPS16B form a high MW complex in mammalian cells

Studies using blue native polyacrylamide gel electrophoresis (BN-PAGE) were performed as described previously (42). This method preserves noncovalent interactions between proteins within multimeric complexes as well as the native folded state of most proteins (43). Immunoblotting with antibodies for endogenous proteins revealed that the complex isolated from both human embryonic kidney 293 (HEK293) and DAMI (megakaryoblastic DAMI cell line) cells contained both VPS33B and VPS16B and comigrated with the 480 kDa marker, making it larger than the combined MWs of 70.6 kDa for VPS33B and 57 kDa for VPS16B (Fig. 1*A*). This indicates the VPS33B–VPS16B complex is larger than a heterodimer. To determine the robustness of the interaction of complex components, affinity-tagged VPS33B and VPS16B were cotransfected into HEK293 cells, and each tagged protein was found to be capable of coimmunoprecipitating (co-IP) the other, confirming the presence of both proteins in the complex (Fig. 1*B*). As in untransfected HEK293 cells (Fig. 1*A*), cotransfected Myc-VPS16B/VPS33B-3xFLAG and Myc-VPS33B/VPS16B-3xFLAG formed a predominant ∼480 kDa complex and smaller amounts of a >720 kDa complex (Fig. 1*C*).

Two or more copies of VPS33B and VPS16B are present in the complex

To determine whether multiple copies of VPS33B and/or VPS16B are present in the complex, we utilized differentially tagged proteins selectively expressed in HEK293 cells, as shown in Figure 2, *A–D*. Hemagglutinin (HA)-VPS33B, Myc-VPS16B, and VPS16B-FLAG coexpressed in HEK293 cells (Fig. 2*A*) revealed that VPS16B-FLAG could co-IP Myc-VPS16B (Fig. 2*B*). Similarly, when HA-VPS33B, Myc-VPS16B, and VPS33B-FLAG were cotransfected (Fig. 2*C*), VPS33B-FLAG could co-IP HA-VPS33B (Fig. 2*D*). These results

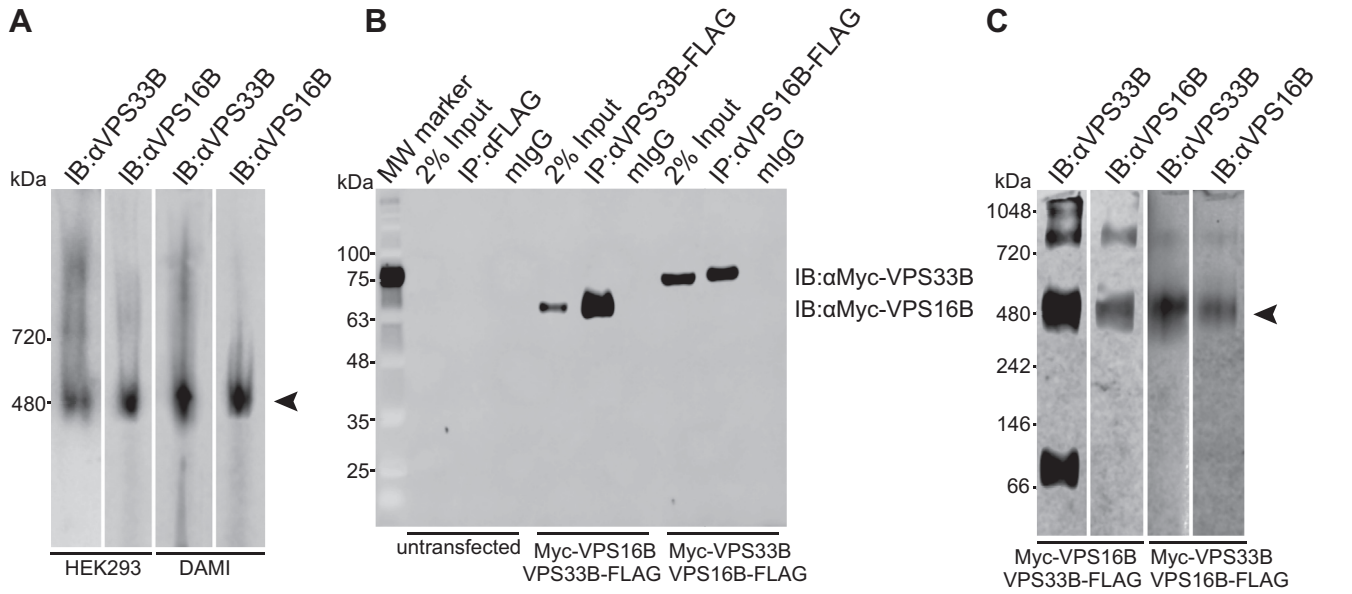

Figure 1. VPS33B and VPS16B form a high molecular weight complex. *A*, immunoblot analysis of HEK293 and DAMI cell lysates subjected to BN-PAGE detected native protein complexes (*arrowhead*) containing VPS33B and VPS16B that comigrated with 480 kDa marker. *B*, SDS-PAGE immunoblot showing co-IPs with anti-FLAG antibody of lysates from HEK293 cells cotransfected with Myc-VPS16B or Myc-VPS33B, plus VPS33B-3xFLAG or VPS16B-3xFLAG, respectively, probed with anti-Myc antibody. *C*, BN-PAGE immunoblots of co-IP experiments using anti-FLAG antibody and lysates from HEK293 cells cotransfected with Myc-VPS16B plus VPS33B-3xFLAG or Myc-VPS33B plus VPS16B-3xFLAG. Blots show Myc-tagged subunit co-IPs with FLAG-tagged subunit, indicating consistent formation of VPS33B–VPS16B complex comigrating with 480 kDa marker (*arrowhead*). BN-PAGE, blue native polyacrylamide gel electrophoresis; co-IP, coimmunoprecipitation; DAMI, megakaryoblastic DAMI cell line; HEK293, human embryonic kidney 293 cell line; VPS, vacuolar protein sorting protein.

indicate that in mammalian cells, both native and tagged VPS33B and VPS16B form a large stable complex containing more than one copy of each protein.

Human VPS33B and VPS16B expressed in yeast also form a high MW complex

To delineate the structure of the VPS33B–VPS16B complex, we required the sizeable amounts of protein typically generated *via* cellular expression systems. When expressed in *Escherichia coli*, we found that VPS33B and VPS16B were mostly present in insoluble inclusions, and whereas expression in Sf9 and Sf21 insect cells using baculovirus yielded stable complex, the yield was insufficient for structural analysis. We then found that human VPS33B and VPS16B can be expressed at higher levels in *S. cerevisiae* using the pBEVY-T vector, which contains a constitutive bidirectional glyceraldehyde-3-phosphate dehydrogenase-alcohol dehydrogenase I fused promoter suitable for coexpression of two proteins at similar levels (44). Untagged VPS33B and VPS16B-3xFLAG purified from yeast using FLAG affinity purification followed by anion exchange chromatography revealed the expected MWs on BN-PAGE immunoblots (Fig. 3*A*) and showed no significant impurities on Coomassie blue-stained gels (Fig. 3*B*). The expected predominant ∼480 kDa complex was observed on a stained BN-PAGE gel (Fig. 3*C*), from which the band was extracted and after trypsin digestion analyzed by mass spectrometry, which detected primarily VPS33B and VPS16B (Table S1). The only additional protein detected was the yeast actin-binding protein YFR016C. Only two YFR016C peptides with total spectral count of two were detected compared with spectral counts of more than 200 for VPS33B and VPS16B peptides; therefore, this is probably not a specific interactor with human VPS33B–VPS16B. VPS33B–VPS16B-3xFLAG affinity purified from yeast was also examined using circular dichroism, which relies on differential absorption of left- and right-handed circularly polarized light of varying wavelengths by protein secondary structures and can be used to assess the folded state of protein (45). The VPS33B–VPS16B-3xFLAG complex was observed to be well folded and primarily alpha helical (Fig. 3*D*).

VPS33B and VPS16B form a 315 kDa MW complex

The size of VPS33B–VPS16B has not previously been determined, beyond an estimate of the hydrodynamic radius of a recombinant complex determined by SEC (41). We used SEC–MALS to determine the MW of purified VPS33B–VPS16B (Figs. 3*E* and S1), detected in a peak fraction confirmed by immunoblotting to contain VPS33B and VPS16B (Fig. 3*F*). Results from analysis of three independent purifications gave MW estimates for VPS33B–VPS16B of 310 kDa ± 9%, 327 kDa ± 3.3%, and 310 kDa ± 0.4%. These values give an average MW of ∼315 kDa, which is larger than the minimal size predicted from co-IP experiments that indicated the presence of at least two copies each of VPS33B and VPS16B (Fig. 2) for a total minimum MW of ∼261 kDa (VPS33B: 70.6 × 2 = 141.2 kDa and VPS16B-3xFLAG: 60.8 × 2 = 121.6 kDa).

The VPS33B–VPS16B complex contains two copies of VPS33B and three copies of VPS16B

To determine the ratio of components within VPS33B–VPS16B, we expressed both proteins in yeast with short

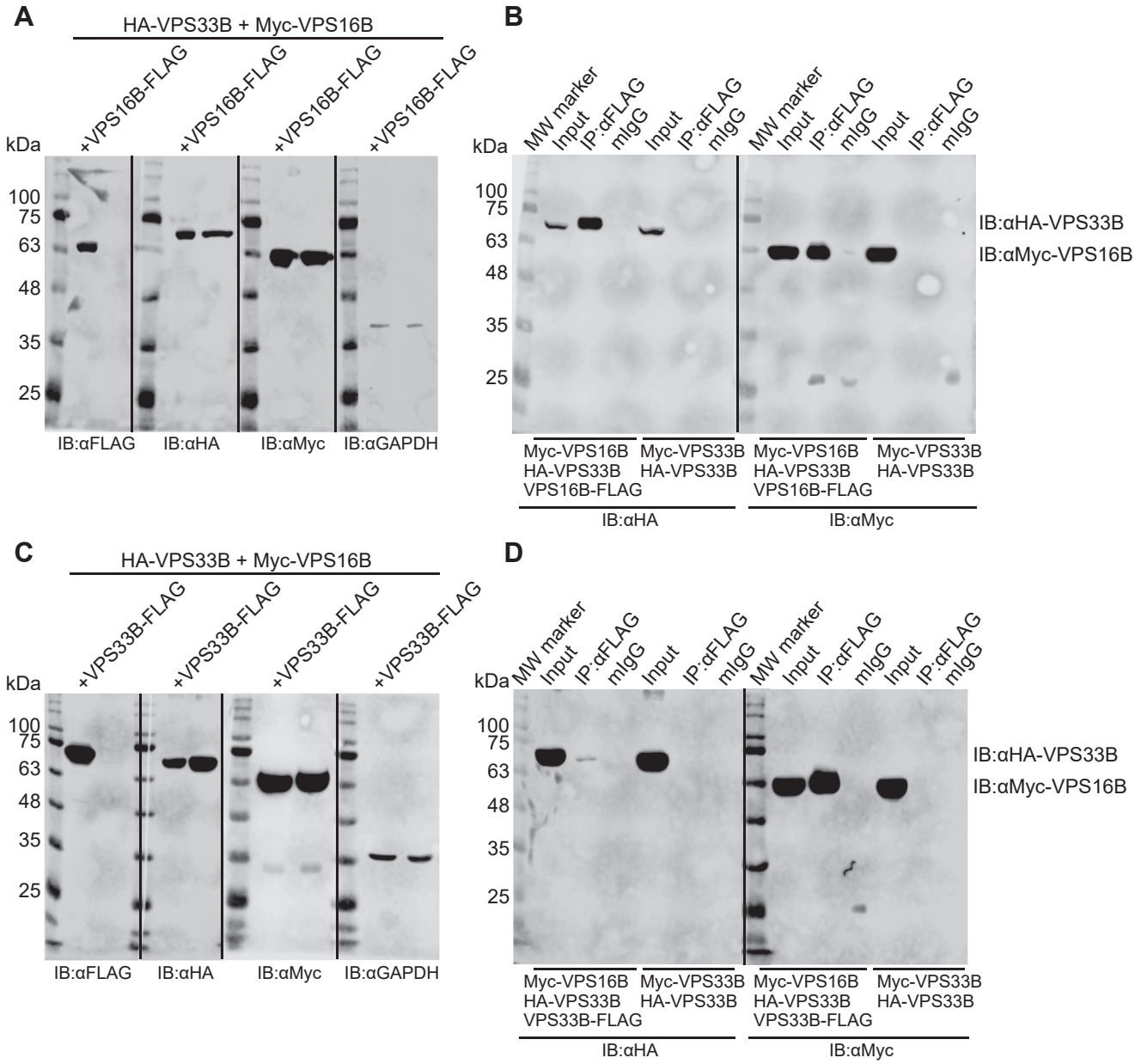

Figure 2. The VPS33B–VPS16B complex contains multiple copies of each component. *A–D*, SDS-PAGE immunoblots show differentially tagged VPS33B and VPS16B expressed in transfected HEK293 cells can co-IP a second copy of each protein. *A*, probing for FLAG, HA, Myc, and GAPDH (*bottom*) of lysates from HEK293 cells cotransfected with HA-VPS33B + Myc-VPS16B, and with/without VPS16B-FLAG as indicated. *B*, in lysates from triple-transfected cells, anti-FLAG antibody co-IP's HA-tagged VPS33B and Myc-tagged VPS16B, confirming at least two copies of VPS16B in the complex. *C*, probing of lysates from cells cotransfected with HA-VPS33B + Myc-VPS16B, and with/without VPS33B-FLAG. *D*, in lysates from triple-transfected cells, anti-FLAG antibody co-IP's HA-tagged VPS33B and Myc-tagged VPS16B, confirming at least two copies of VPS33B in the complex. co-IP, coimmunoprecipitation; HA, hemagglutinin; HEK293, human embryonic kidney 293 cell line; VPS, vacuolar protein sorting protein.

N-terminal HA tags and confirmed recovery of affinity-purified complex by SDS-PAGE (Fig. 4*A*). Immunoblots of serially diluted samples were probed with primary anti-HA antibody and secondary Alexa-488-labeled antibody, and nonsaturated sets of bands were quantified by scanning (Fig. 4, *B* and *C*). We observed that the VPS33B band (band 1, *upper*) represented 39.1% of the signal and the VPS16B band (band 2, *lower*) represented 60.9%, indicating a 2:3 ratio of VPS33B to VPS16B in the complex. The calculated MW of 324 kDa containing two copies of VPS33B (141.2 kDa) and three copies of VPS16B-3xFLAG (182.4 kDa) is comparable to the SEC–MALS determined average MW of ∼315 kDa.

The VPS33B–VPS16B complex has a two-lobed overall structure

We pursued structural determination by negative-staining EM and cryo-EM. Attempts to perform high-resolution cryo-EM with purified complexes were unsuccessful since the complexes became heterogeneous and produced very low-resolution 2D and 3D classes. It is likely that this was due to

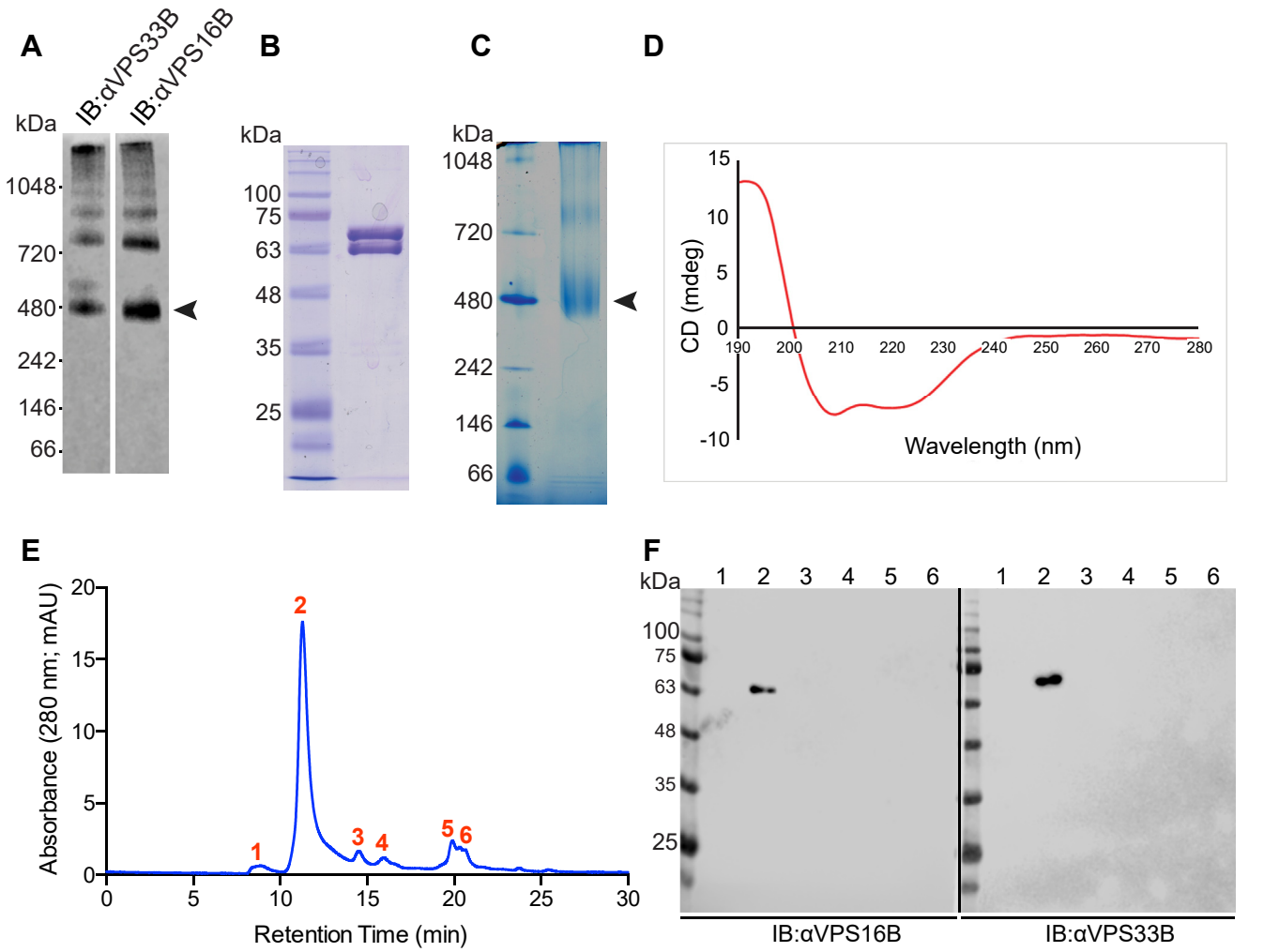

Figure 3. Human VPS33B–VPS16B complex expressed in yeast is stable and well folded with a molecular weight of approximately 315 kDa. *A*, BN-PAGE immunoblots probed for VPS33B and VPS16B show the presence of both in human VPS33B–VPS16B-3xFLAG complexes affinity purified from yeast; major band comigrates with 480 kDa marker (*arrowhead*) as in HEK293 and DAMI cell lysates (Fig. 1*A*). *B*, Coomassie blue–stained SDS-PAGE gel indicates VPS33B and VPS16B are the only proteins present in purified complex, also shown in native form. *C*, on stained BN-PAGE gel. *D*, circular dichroism analysis of purified complex indicates mostly helical secondary structure. *E*, Representative SEC-MALS chromatogram for purified complex. *F*, SDS-PAGE immunoblots detected VPS33B and VPS16B in the major peak (fraction 2); results yielded a mean calculated molecular weight of 315 kDa for the complex (see Fig. S1 for light scattering data). BN-PAGE, blue native polyacrylamide gel electrophoresis; DAMI, megakaryoblastic DAMI cell line; HEK293, human embryonic kidney 293 cell line; VPS, vacuolar protein sorting protein.

the cryo-EM sample preparation causing unfavorable interactions between the VPS33B–VPS16B-3xFLAG complex and the air–water interface and/or flexibility within the complex. Flexibility was also an obstacle to initial structural determination of the intact HOPS complex by cryo-EM, requiring crosslinking and negative-staining EM (46). We therefore focused our efforts on negative-staining EM, utilizing glutaraldehyde crosslinking to stabilize the complex. Negative-staining EM of the VPS33B–VPS16B complex revealed a two-lobed configuration, approximately 15 nm along the major axis. 2D classification of complexes revealed a slight bend between the two lobes. The complex appears to contain two ball-like structures connected by a thinner stalk (Fig. 5, *A* and *B*). Validation of this structure came from SAXS of affinity purified VPS33B–VPS16B-3xFLAG (Fig. S2, *A* and *B*). The results revealed VPS33B–VPS16B has a radius of gyration of 7.27 ± 0.14 nm and hydrodynamic radius of 9.38 ± 0.18 nm, dimensions consistent with our negative-staining results.

Localization of VPS33B molecules within the complex

To localize VPS33B, we tagged the C terminus with a biotinylation signal to allow attachment of avidin, which can be resolved by negative-staining EM of purified VPS33B–VPS16B. VPS33B containing the C-terminal biotinylation signal formed a complex with VPS16B that could be purified from yeast, as shown in SDS-PAGE and BN-PAGE gels (Fig. 6, *A* and *B*). Subsequent attachment of avidin tetramers and negative-staining EM revealed avidin extensions on opposing ends of the bilobed complex, indicating the positioning of VPS33B molecules within the complex in a trans orientation (Fig. 6, *C* and *D*).

N- and C-terminal regions of VPS16B are not required for the VPS33B–VPS16B complex

To determine regions of VPS33B and VPS16B required for complex formation, we made a series of truncations and

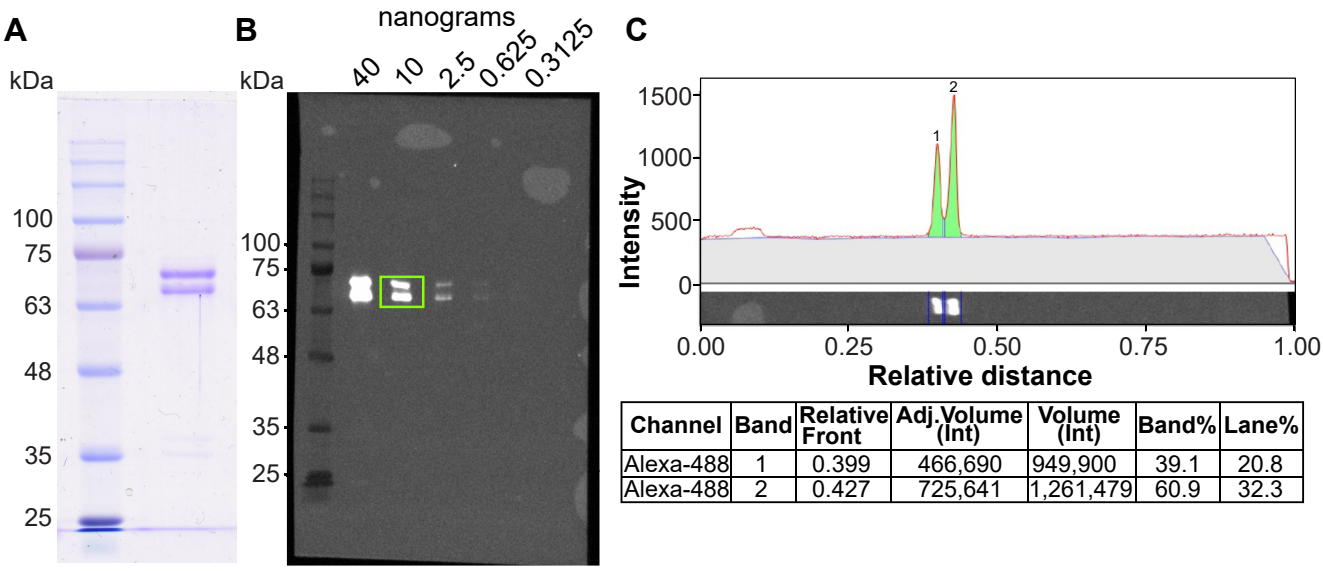

Channel	Band	Relative Front	Adj.Volume (Int)	Volume (Int)	Band%	Lane%
Alexa-488	1	0.399	466,690	949,900	39.1	20.8
Alexa-488	2	0.427	725,641	1,261,479	60.9	32.3

Figure 4. The VPS33B–VPS16B complex contains two VPS33B and three VPS16B proteins. *A*, SDS-PAGE gel of HA-VPS33B–HA-VPS16B-3xFLAG complex purified from yeast lysate *via* FLAG affinity purification and anion exchange chromatography. *B*, serially diluted samples of complex (total protein shown for each lane) were blotted and probed with monoclonal anti-HA primary antibody and Alexa Fluor 488–conjugated secondary antibody; *box* indicates 10 ng bands used for quantification (see the *Experimental procedures* section). *C*, analysis of fluorescence signal showed 39.1% of total corresponded to HA-VPS33B and 60.9% to HA-VPS16B-3xFLAG, indicating a 2:3 ratio of these proteins in the complex. HA, hemagglutinin tag; VPS, vacuolar protein sorting protein.

assessed complex assembly. We observed that truncations in VPS33B (VPS33B [202–617], VPS33B [322–617], VPS33B [1–360], and VPS33B [1–401]) were not tolerated, resulting in lack of expression in yeast. However, deletions in VPS16B (VPS16B [143–493], VPS16B [143–316]), when expressed with full-length VPS33B, were affinity purified (Fig. 7, *A* and *B*). Complexes containing both VPS16B truncations could be isolated on BN-PAGE (Fig. 7, *C* and *D*) and were able to form bilobed complexes similar to intact VPS16B (Fig. 7, *E* and *F*). We confirmed that the composition of two copies of VPS33B and three copies of truncated VPS16B was maintained in these complexes (Fig. S3). These data indicate that the core portion of VPS16B, VPS16B (143–316), is required for VPS33B–VPS16B interaction in the complex. The N and C termini of VPS16B may have additional roles in complex function.

ARC-causing L30P variant in VPS33B abrogates complex formation

ARC-causative single amino acid substitutions of VPS33B are cataloged in the Leiden Open Variation Database (https://grenada.lumc.nl/LSDB_list/lsdbs/VPS33B) (47). When the ARC-causing VPS33B variant L30P was coexpressed with VPS16B-3xFLAG and protein was FLAG affinity purified, we observed the absence of the typical VPS33B band together with the appearance of a prominent ∼70 kDa band on SDS-PAGE (Fig. 8*A*), which mass spectrometry identified as yeast HSP70-family proteins (Table S2). Immunoblotting confirmed the absence of both VPS33B and VPS16B-FLAG (Fig. 8, *B* and *C*) in coexpressing yeast cell lysates, consistent with loss of both proteins in humans with this variant (48), suggesting that the L30P region of VPS33B is important for stable complex formation. In contrast, similar examination of the ARC-associated VPS33B variants S243F and H344D showed they could be recovered when coexpressed with VPS16B-3xFLAG in yeast (Fig. 8*A*), although immunoblotting indicated slightly lower expression of VPS33B and VPS16B (Fig. 8, *B* and *C*). Both variants formed complexes with VPS16B detected by BN-PAGE (Fig. 8*D*), which showed the expected bilobed structure when assessed by negative-staining EM (Fig. 8, *E* and *F*). The interaction of VPS16B (VIPAS39) with S243F VPS33B has been suggested in a previous study (49); however, interaction with the H344D variant has not been reported.

Proposed structure of the VPS33B–VPS16B complex

To refine our model of the 2:3 VPS33B–VPS16B complex, we combined our EM data for the overall bilobed structure (Fig. 5) and the location of VPS33B subunits (Fig. 6*D*) with predicted structures derived from the AlphaFold Protein Structure Database (https://alphafold.ebi.ac.uk/), generated *via* an artificial intelligence system that has produced highly accurate 3D protein structure predictions for 200 million proteins from amino acid sequences (50–52). The structure for VPS33B (https://alphafold.ebi.ac.uk/entry/Q9H267) contains several alpha helices folded into a ball (Fig. 9*A*, *left upper panel—red dots* indicate C-terminal serine residues) where the per-residue confidence score (pLDDT) is very high (pLDDT >90) as indicated by the large proportion of *blue* in the ribbon structure. Other regions (indicated in *yellow*) have low to very low confidence, and we modeled these next to each other in the proposed trans arrangement of VPS33B proteins. The predicted structure for VPS16B (VIPAS39; https://alphafold.ebi.ac.uk/entry/Q9H9C1) is elongate (Fig. 9*A*, *lower left*) with a core region of alpha helices at very high confidence (outlined in *green*), and a less structured N-terminal region (amino acids 1–152) with low to very low confidence (shown in *yellow*). Guided by this information and a 3D volume derived from our

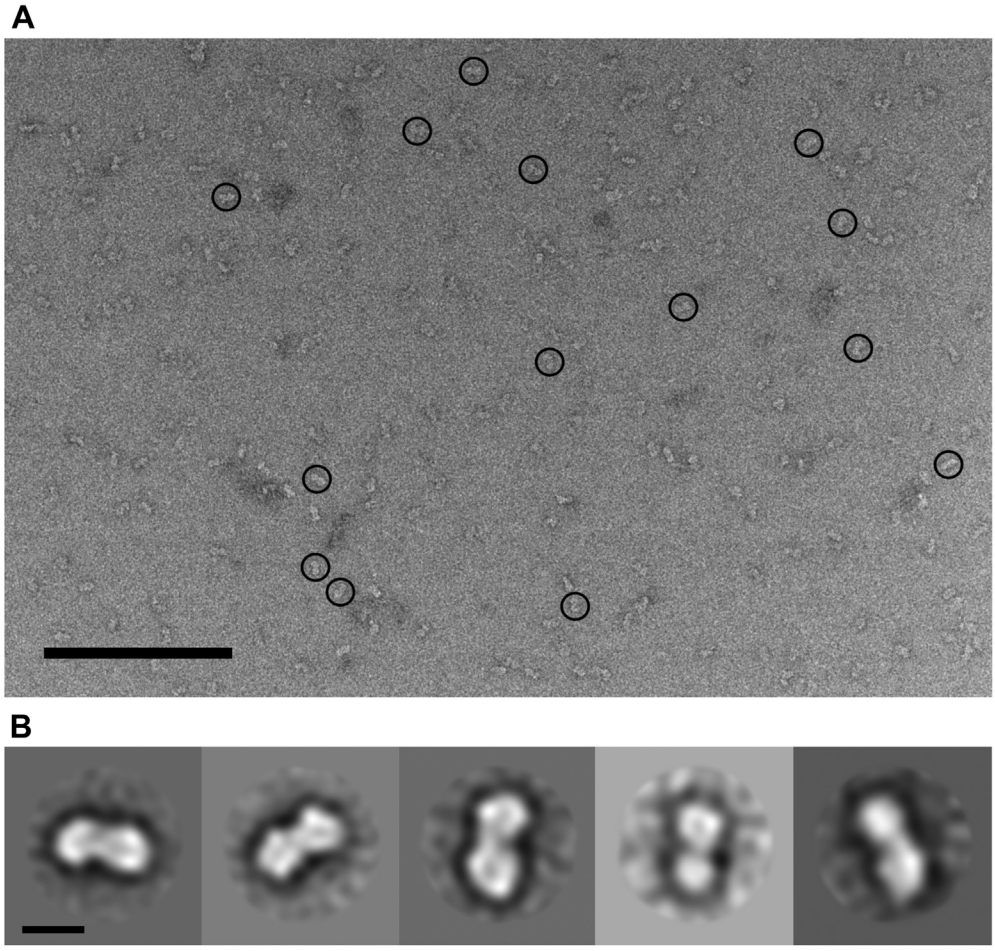

Figure 5. Negative-staining EM of VPS33B–VPS16B complex. *A*, representative micrograph of negative-stained glutaraldehyde-crosslinked purified VPS33B–VPS16B-3xFLAG complex; *circles* indicate representative particles used for 2D class averaging. Micrographs collected at 25,000× magnification with image pixel size of 2.61 Å; bar represents 200 nm. *B*, 2D class averages generated from 407 particles reveal an elongated two-lobed complex structure; bar represents 10 nm. VPS, vacuolar protein sorting protein.

EM data (Fig. 9*A*, *right panel top*), we propose that in the VPS33B–VPS16B complex, two well-folded VPS33B molecules comprise either end in an opposing trans orientation, whereas three VPS16B molecules are located between them (Fig. 9*A*, *right panel bottom*).

Location of VPS16B (143–316) and ARC amino acid variants in VPS33B

We depicted the N- and C-terminal truncation of VPS16B superimposed on the AlphaFold predicted structure (Fig. 9*B*, *turquoise* where deleted portions are *pink*). Since the structure of VPS33B is predicted with high confidence, we localized the Leu30Pro, Ser243Phe, and His244Asp amino acid variants into the AlphaFold model (Fig. 9*C*). Here, the introduction of a proline at position 30 somehow disrupts the whole complex by either dramatically altering the folding of VPS33B and/or its interaction with VPS16B.

Discussion

ARC syndrome is typically fatal within the first few months of life because of multisystem failure. Organ involvement includes the liver with cholestasis and intrahepatic biliary duct hypoplasia, the kidney with renal tubular acidosis, and Fanconi syndrome (polyuria, aminoaciduria, glycosuria, phosphaturia, and bicarbonate wasting), arthrogryposis multiplex congenita characterized by immobility of the limbs with fixation of multiple joints and muscle wasting, dysmorphic features, failure to thrive, and bleeding because of platelet dysfunction (47). Two genes have been linked to this disease: *VPS33B* (Online Mendelian Inheritance in Man: 608552) and *VIPAS39* (Online Mendelian Inheritance in Man: 613401) encoding, respectively, VPS33B and VPS16B (alternative VIPAR or VIPAS39) (1, 2). Despite the vital functions that these proteins play in multiple tissues, likely affecting intracellular vesicular trafficking, little is known about the details of their structure and function. Observations that VPS33B and VPS16B bind to each other, and that loss of either affected the expression of VPS33B and VPS16B, suggested that these proteins stabilize each other in cells (5, 48). The first clue that these proteins bind each other came from our studies of cell isolates run on BN-PAGE, revealing a predominant large MW complex (comigrating with ~480 kDa marker) containing both VPS33B and VPS16B (Fig. 1). Differential tagging and co-IP results subsequently

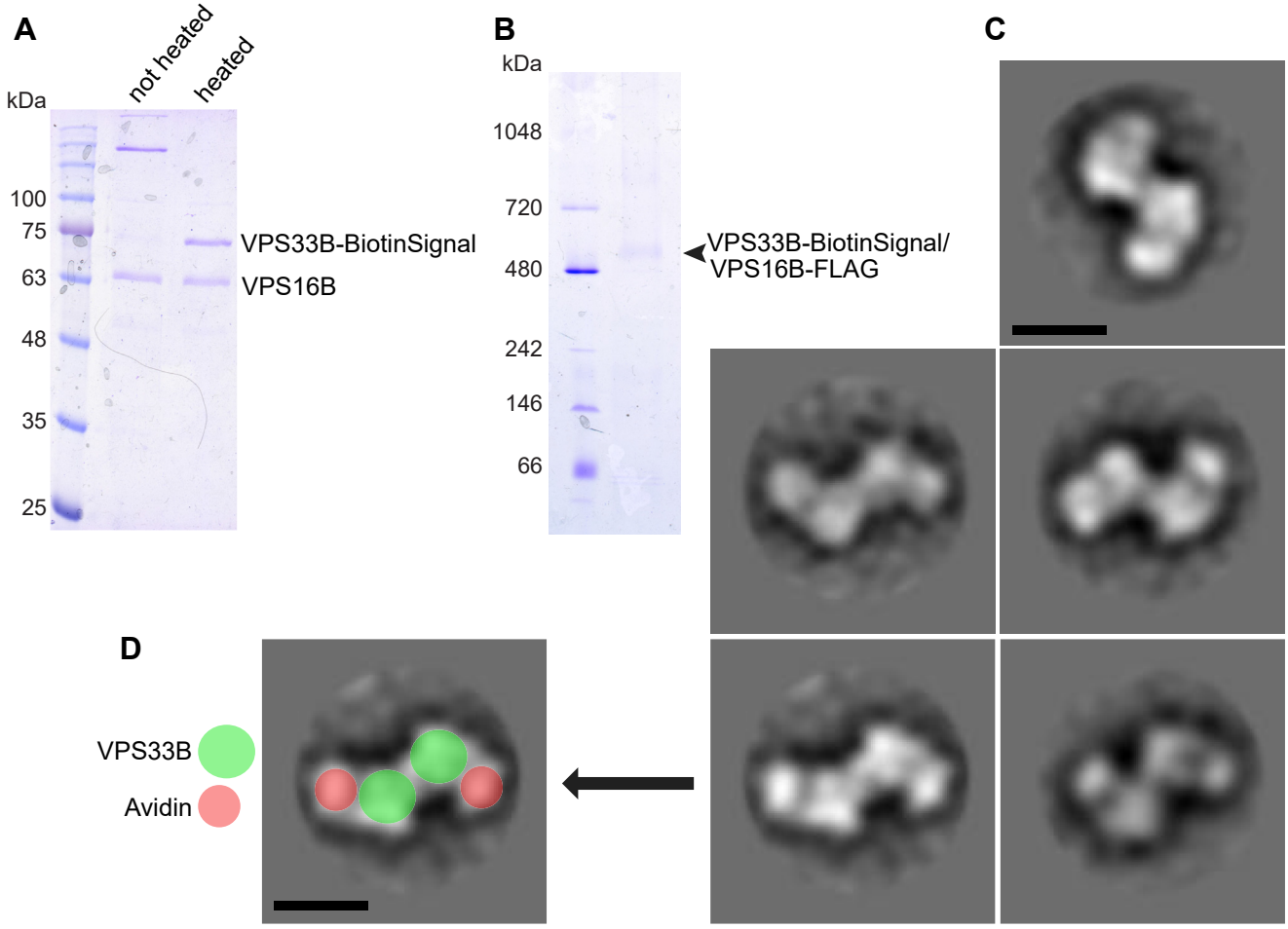

Figure 6. Localization and orientation of VPS33B within complex *via* avidin labeling of biotinylated VPS33B. *A*, SDS-PAGE gel showing avidin-labeled VPS33B–VPS16B; avidin binding to biotinylated VPS33B was disrupted by preheating the sample to 95 °C for 5 min. *B*, BN-PAGE gel shows that addition of the biotinylation signal does not disrupt formation of VPS33B–VPS16B complex (*arrowhead*). *C*, 2D class averages derived from negative-staining EM of crosslinked avidin-labeled VPS33B–VPS16B show avidin bound to opposing sides of the broad lobes of the complex. Classes were generated from 234 particles. The scale bar represents 10 nm. *D*, 2D class showing representation of avidin and VPS33B overlaid to indicate position of VPS33B subunits (71 kDa native protein + 8 kDa biotinylation signal) and avidin (tetramer with total molecular weight of 67 kDa). The scale bar represents 10 nm. BN-PAGE, blue native polyacrylamide gel electrophoresis; VPS, vacuolar protein sorting protein.

indicated the presence of more than one copy of each protein in this complex (Fig. 2).

We determined that human VPS33B and VPS16B cannot be produced in sufficient quantities in bacteria or insect cells for biochemical characterization. However, a yeast expression system using a bidirectional promoter expressing human untagged VPS33B and C-terminally tagged VPS16B allowed us to directly assess VPS33B–VPS16B complex formation by analyzing affinity-purified protein complexes. Since only VPS16B is FLAG tagged, isolation of the complex depends on VPS33B binding to VPS16B in yeast. We found that VPS16B cannot be isolated independently of VPS33B (possibly because of proteolysis or other mechanisms), as also observed in humans (48). Therefore, any alterations that disrupted binding between VPS33B and VPS16B would abrogate the ability to isolate either protein from yeast. Using this expression system, we were able to not only evaluate native human VPS33B–VPS16B complex but also the effects of VPS16B truncations and ARC-causing missense variants in VPS33B.

While the exact composition of the VPS33B–VPS16B complex was previously undetermined, several models were proposed. These included a HOPS-like class C homolog in endosome–vesicle interaction complex containing one copy each of VPS33B and VPS16B forming a heterodimer (38, 39). However, our observations that native VPS33B and VPS16B in HEK293 or DAMI cells comigrated with the 480 kDa size marker on BN-PAGE (Fig. 1), and that at least two copies of each VPS33B and VPS16B (Fig. 2) may be present, suggested an alternative composition of the VPS33B–VPS16B complex.

Affinity-purified VPS33B–VPS16B subjected to ion exchange chromatography yielded a sample containing only VPS33B and VPS16B, as assessed *via* SDS-PAGE (Fig. 3*B*). The same sample subjected to BN-PAGE revealed a predominant complex comigrating with the 480 kDa marker (Fig. 3, *A* and *C*). Mass spectrometry ruled out binding of additional proteins in the complex (Table S1). The complex was well folded with an alpha-helical configuration as per circular dichroism (Fig. 3*D*). The yeast-purified complex comigrated with the

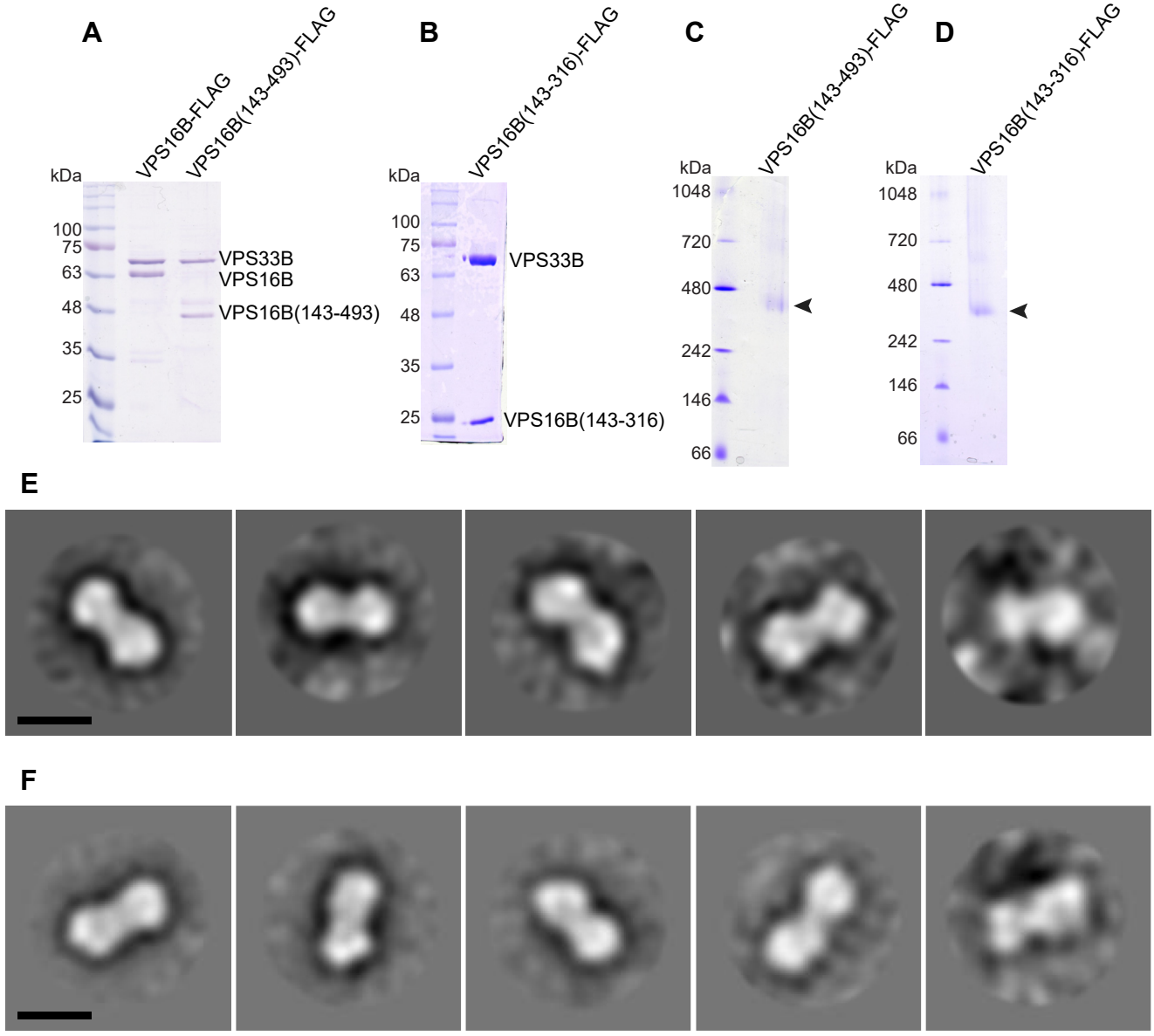

Figure 7. Truncated VPS16B forms a stable complex with VPS33B. *A*, Coomassie blue–stained SDS-PAGE gel comparing purified VPS33B–VPS16B complex containing wildtype or N-terminal truncated VPS16B. *B*, SDS-PAGE gel of complex containing VPS33B and amino acids 143 to 316 of VPS16B. *C*, BN-PAGE gel of VPS33B in complex with amino acids 143 to 493 of VPS16B (*arrowhead*); truncation does not appear to disrupt complex formation. *D*, BN-PAGE gel of VPS33B in complex with amino acids 143 to 316 of VPS16B (*arrowhead*); truncation does not appear to disrupt complex formation. *E*, 2D class averages from negative-staining EM of crosslinked VPS33B–VPS16B(143–493) complex showing a two-lobed structure similar to full-length complex (Fig. 5*B*), indicating the stable association of subunits when N terminus of VPS16B is absent. Classes were generated from 308 particles. *F*, 2D class averages from negative-staining EM of crosslinked VPS33B–VPS16B(143–316) complex showing a two-lobed structure similar to full-length complex, indicating the stable association of subunits when N- and C-terminal regions of VPS16B are absent. Classes were generated from 424 particles. The scale bars represent 10 nm. VPS, vacuolar protein sorting protein.

native VPS33B–VPS16B complex near the 480 kDa marker on BN-PAGE, suggesting that the VPS33B–VPS16B complex is distinct from previously proposed models (38, 39).

To determine a more precise MW of the VPS33B–VPS16B complex, we employed SEC–MALS, revealing an average MW of 315 kDa (Figs. 3, *E* and *F* and S1). This is larger than the predicted ∼257 kDa for a complex containing two copies each of VPS33B and VPS16B, thus requiring further analysis. Quantitative immunoblotting with HA-tagged proteins revealed that there are two copies of VPS33B and three copies of VPS16B in the VPS33B–VPS16B complex (Fig. 4). This complex has a calculated MW of 321 kDa, in agreement with the SEC–MALS analysis.

Visualization of the structure of the VPS33B–VPS16B complex was facilitated by negative-staining EM, where we observed a two-lobed configuration (Fig. 5). This apparently symmetrical structure indicated that the lobes likely had a similar composition. Localization of VPS33B within the complex was achieved by the addition of a biotinylation signal at the C terminus that allowed subsequent avidin binding (53). Visualization *via* negative-staining EM revealing avidin present in each lobe in a trans orientation (Fig. 6, *C* and *D*), indicating

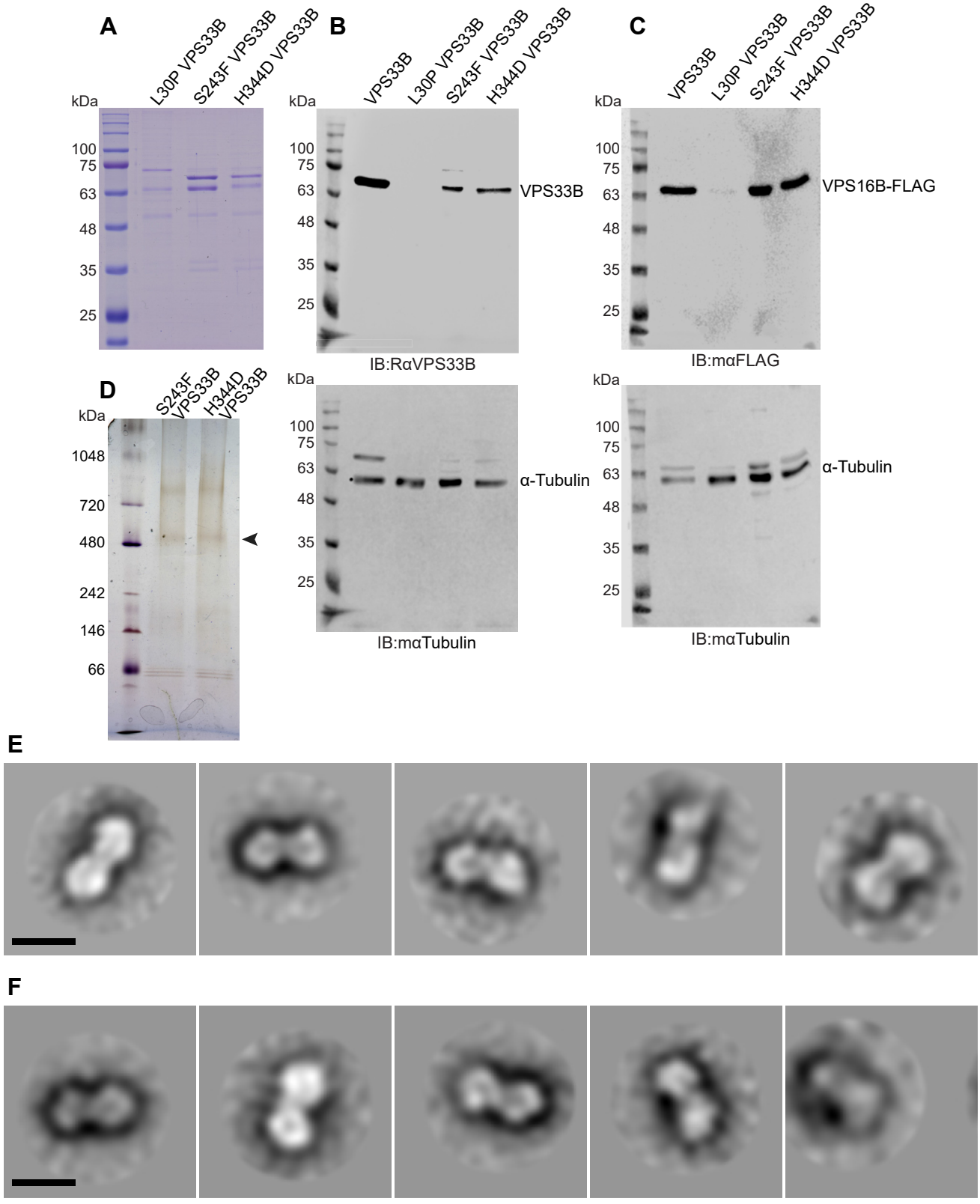

Figure 8. Effects of ARC-syndrome causative VPS33B variants L30P, S243F, and H344D on complex formation. *A*, SDS-PAGE gel of complexes containing VPS33B L30P, S243F, and H344D purified from yeast shows VPS33B is mostly absent in the L30P sample and VPS16B is also reduced. *B*, immunoblotting for VPS33B in yeast lysates expressing VPS33B wildtype, L30P, S243F, and H344D along with wildtype VPS16B-3xFLAG show VPS33B is undetectable in the L30P lysate. *C*, immunoblotting for VPS16B-3xFLAG in yeast lysates from cultures expressing VPS33B wildtype, L30P, S243F, and H344D shows FLAG signal is weak in the L30P lysate. For (*B*) and (*C*), nitrocellulose membranes were blotted for α-tubulin as loading control without stripping. *D*, silver-stained BN-PAGE gel of complexes containing VPS33B S243F or H344D showing that these variants do not disrupt complex formation. Complex indicated by *arrowhead*. *E*, 2D class averages from negative-staining EM of VPS33B–VPS16B-3xFLAG complexes containing VPS33B S243F mutation. Classes generated from 257 particles. The scale bar represents 10 nm. *F*, 2D class averages from negative-staining EM of VPS33B–VPS16B-3xFLAG complexes containing VPS33B H344D mutation. Classes generated from 259 particles. The scale bar represents 10 nm. ARC, arthrogryposis, renal dysfunction, and cholestasis; BN-PAGE, blue native polyacrylamide gel electrophoresis; VPS, vacuolar protein sorting protein.

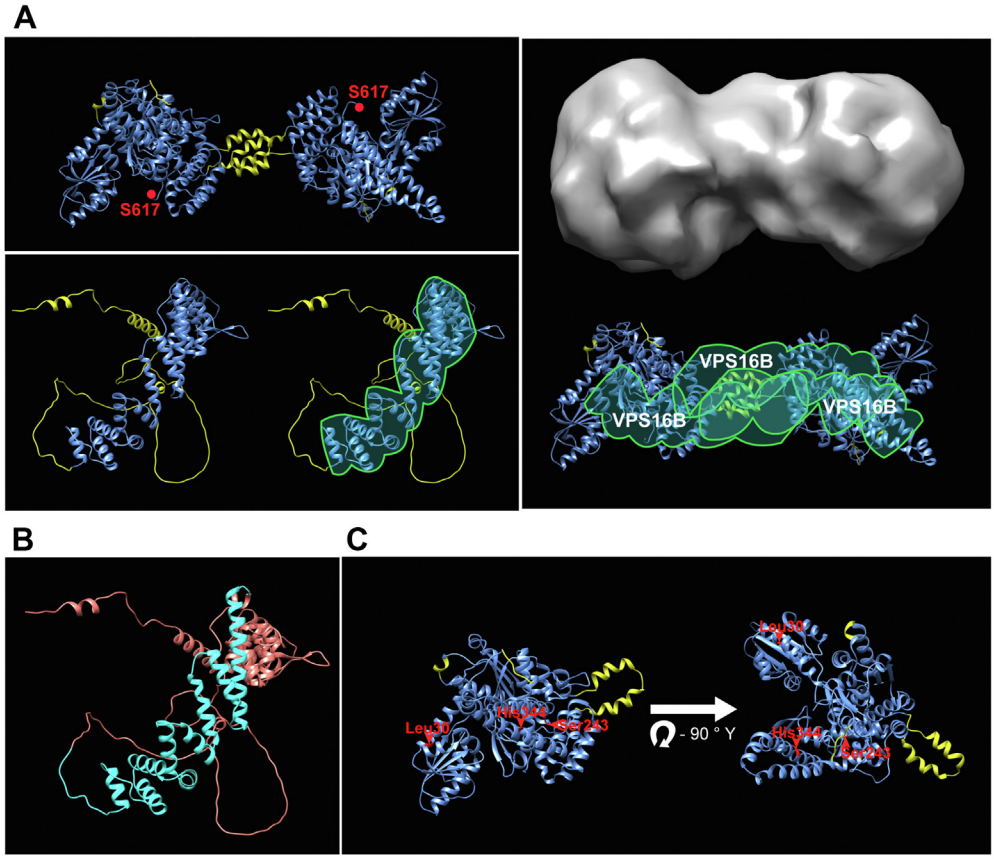

Figure 9. Proposed model of the VPS33B–VPS16B complex. *A*, *top left*, two copies of the AlphaFold predicted VPS33B structure (https://alphafold.ebi.ac.uk/entry/Q9H267) arranged in trans, consistent with our structural data (Fig. 6; C-terminal serine 617 highlighted in *red*). *Bottom left*, two copies of the AlphaFold VPS16B structure (https://alphafold.ebi.ac.uk/entry/Q9H9C1) with high-confidence region highlighted in *green outline*. *Right*, VPS33B–VPS16B complex 3D volume (*gray*) generated from negative-staining EM data (Fig. 5), above proposed model of the complex assembled from two VPS33B molecules bridged by three VPS16B. *B*, AlphaFold predicted structure of VPS16B with highlighted amino acids 143 to 316 (*turquoise*) we have identified as necessary for complex formation. *C*, AlphaFold predicted structure of VPS33B showing ARC-causing amino acid changes L30P, S243F, and H344D highlighted in *red*; the structures are rotated −90° along the *Y*-axis relative to each other. For AlphaFold predicted structures in (*A*) and (*C*), *blue ribbon* indicates per-residue confidence scores >70 (confident and very confident), and *yellow ribbon* indicates per-residue confidence scores <70 (low and very low confidence). ARC, arthrogryposis, renal dysfunction, and cholestasis; VPS, vacuolar protein sorting protein.

that molecules of VPS33B form the cores of each lobe with their respective C termini oriented outward. From this, we propose that three molecules of VPS16B bind the VPS33B present in each lobe. In agreement with this model is the observation that in human ARC syndrome loss of VPS33B results in a concomitant loss of VPS16B, as we recently showed (48). Conversely, loss of VPS16B results in reduced but not absent VPS33B in cells (5). This is in keeping with our proposed model where VPS33B forms the core of the complex with VPS16B bridging the two lobes.

We further investigated how VPS16B fits into VPS33B–VPS16B by examining the effects of VPS16B truncations on the two-lobed structure of the complex expressed in yeast. Surprisingly, truncation of either the N-terminal 1 to 142 amino acids, or both the N-terminal 1 to 142 and C-terminal 317 to 493 amino acids of VPS16B, permitted formation of complexes with the same composition as full-length VPS16B (Figs. 7 and S3). The two-lobed VPS33B–VPS16B complex also appeared intact when visualized per negative-staining EM (Fig. 7, *E* and *F*). As mentioned, truncated VPS16B containing only amino acids 143 to 316 (depicted in Fig. 9*B*) was able to form the two-lobed VPS33B–VPS16B complex (Fig. 7*F*), suggesting that a minimal portion of VPS16B is required for complex formation. The data suggest that the N and C termini of VPS16B are not required for complex formation but may have roles in vesicular trafficking functions in cells.

To assess how known ARC missense variants may affect the VPS33B–VPS16B complex, we introduced specific variants into our yeast expression system. We observed that VPS33B containing the L30P variant abrogated complex formation (Fig. 8, *A*–*C*). Whether this amino acid change causes an unstable VPS33B conformation, or whether it affects VPS16B binding, is not known. Two ARC-associated VPS33B variants, S243F and H344D, were expressed in yeast (Fig. 8*A*), albeit at lower concentrations compared with normal VPS33B (Fig. 8, *B* and *C*). Both formed the 480 kDa complex (BN-PAGE, Fig. 8*D*) that showed a two-lobed structure when assessed by negative-staining EM (Fig. 8, *E* and *F*). These results suggest that these VPS33B ARC variants likely interfere with VPS33B–VPS16B complex function rather than complex formation.

Predicted protein structures obtained *via* AlphaFold allowed us to approximately model the 2:3 VPS33B–VPS16B complex

into the two-lobed structure derived from EM data (Fig. 9*A*), with the orientation of the two VPS33B subunits indicated by our avidin-tagging data. Each of these contains multiple alpha helices folded into a ball-like structure, which we oriented with their C termini extending outward in opposite directions. The three VPS16B subunits are located at the center of the complex, although their positions have not been accurately determined. Indeed, since only the core portion of VPS16B containing alpha helices is predicted with high confidence, we do not know precisely how this protein interacts with VPS33B or with other copies of itself. Hence, in our proposed model, the VPS16B molecules bridge the VPS33B components in an unspecified manner that leaves one VPS33B exposed at either end of the complex.

VPS33B belongs to the SM protein family, named after *unc-18* in *C. elegans* (54) and *sec1* in *S. cerevisiae* (55). Intracellular membrane fusion enabled by SNAREs depend on SM proteins, where their absence typically abolishes fusion (15, 56–58). X-ray structure determinations of SM proteins delineate a large cleft generated by a helical hairpin, shaping SM proteins like clasps where SNARE binding occurs (15, 57). Understanding the mechanism of SM function has been difficult to define because SM proteins bind to SNAREs in variable ways, including as a clasp binding to four-helix bundle SNAREs in a closed conformation (*e.g.*, Munc18-1/syntaxin-1, Habc domain folded back), open conformation (SM bound to the N-terminal peptide of the syntaxin Habc domain), or *via* trans–SNARE complexes (SNAREpins) (56, 57). A persuasive model incorporating the numerous binding modalities of the SM protein Munc18-1 describes its function as a chaperone (15, 59). Here, Munc18-1 acts as a chaperone and binds syntaxin in a closed conformation to prevent association with other SNAREs. Subsequently, Munc13-1 (tethering two membrane compartments) opens syntaxin, which is followed by VAMP2 binding, thus forming a template complex that is also stabilized by Munc13-1. This results in a half-zippered SNARE complex and ultimately a fully zippered SNARE complex with membrane fusion (15, 59).

VPS33B was recently shown to interact with the SNARE syntaxin 12, where it is also required for the biogenesis of platelet α-granules (60). The VPS33B SNARE-binding cleft is predicted to be adjacent to a key loop containing Arg314–Lys335, and deletion of an equivalent loop involving Ser337–Ala359 in *Caenorhabditis thermophilum*, abrogated SNARE binding (24). Our ability to express VPS33B–VPS16B complexes containing either of the missense variants S243F and H344D could indicate that SNARE binding may be affected by these variants. Human variants of other SM proteins have been linked to disease, including Munc18-1 variants causing early infantile epileptic encephalopathy (61) and VPS45 variants causing a congenital neutrophil defect (62, 63). This emphasizes the fundamental importance of these proteins in cells. The significance of SM proteins is further emphasized by mouse KO studies, where Munc18-1 KO causes death soon after birth (64), Munc18-2 and Munc18-3 KO are both embryonically lethal (65), as is KO of VPS45 (66).

Our proposed model of the VPS33B–VPS16B complex has two VPS33B SNARE clasps pointing in opposing directions, a configuration that has not previously been described for an SM protein. One potential functional implication is that VPS33B–VPS16B may engage two membrane compartments for homotypic membrane fusion (67). Each copy of VPS33B can template one set of fusogenic SNAREs such that one VPS33B–VPS16B complex templates two SNAREpins during membrane fusion (Fig. 10*A*). Alternatively, VPS33B–VPS16B may function in interfaces where multiple membranes are fusing in close proximity where each copy of VPS33B templates SNAREs in a different fusion event (Fig. 10*B*).

Interestingly, neither the N-terminal portions nor the C-terminal portions of VPS16B are required for complex formation, suggesting that these regions have other functions in cells, such as interacting with specific proteins to mediate vesicular trafficking. For example, VPS16B (VIPAS39) was reported to interact with the SM protein VPS45 in *C. elegans* and human cell lines (68). This tethering complex acting in the RAB11 recycling pathway at sorting endosomes was termed FERARI (factors for endosome recycling and Rab interactions) (39), consisting of RAB11FIP5/RABS-5/VPS45/VIPAS39/EHD1 (68), where it is proposed to combine fusion with fission activity. Based on our studies, it is unlikely that these protein interactions occur with the intact VPS33B–VPS16B complex, as it would imply a larger (>315 kDa) MW complex; however, transient interactions cannot be excluded.

Our results indicate that human VPS33B and VPS16B form an approximately 315 kDa complex containing these proteins at a ratio of 2:3 without additional components. The VPS33B–VPS16B complex has a two-lobed structure where VPS33B monomers form the core of each lobe, for which we propose a bidirectional orientation that can potentially facilitate SNARE binding at either end. This is a unique configuration for SM proteins, and we propose that it allows VPS33B–VPS16B to facilitate membrane fusion events that cannot otherwise occur, as indicated by the lethal effects of loss of its expression.

Experimental procedures

HEK293 cell culture and coimmunoprecipitation

Most cotransfections were binary, however, in Figure 2, HEK293 cells were transfected simultaneously with pCMV-HA VPS33B, pCMV-Myc VPS16B, and p3xFLAG-CMV VPS16B (Fig. 2, *A* and *B*) or p3xFLAG-CMV VPS33B (Fig. 2, *C* and *D*) constructs. Transfection of plasmid DNA into cultured cells was performed using PolyPlus JetPrime transfection reagent (VWR; catalog no.: CA89129). HEK293 cells were seeded on 10 cm plates with 10 ml Dulbecco's modified Eagle's medium with 10% fetal calf serum and allowed to grow to 60 to 80% confluence in a 37 °C incubator with 5% CO_2. About 5 μg total DNA was used per plate, with 12 μl JetPrime reagent and 250 μl JetPrime buffer. Media were replaced 4 to 5 h after transfection. About 48 h post-transfection, cells were washed with 5 ml ice-cold PBS and lysed with 2 ml lysis buffer

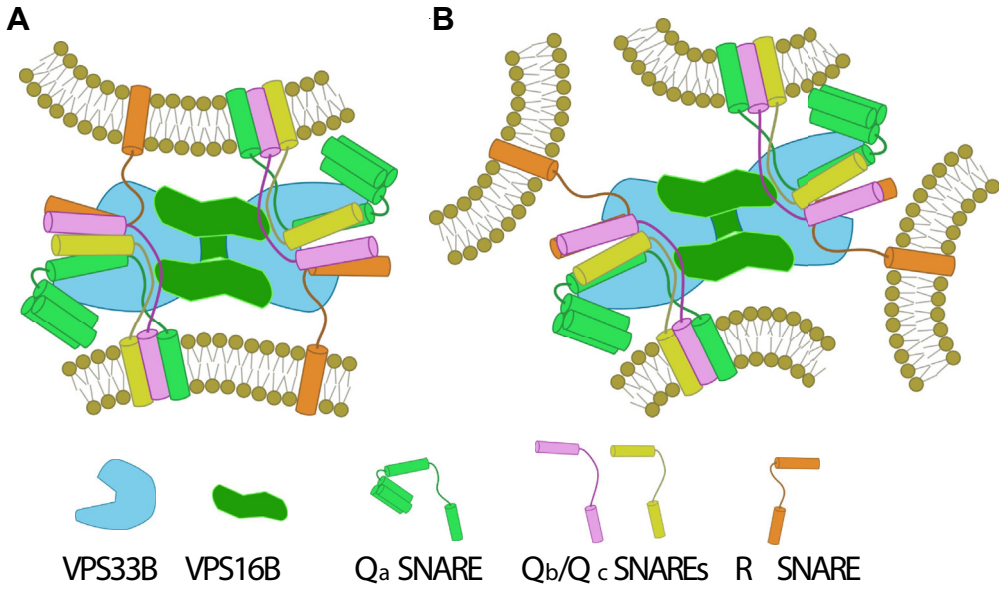

Figure 10. Possible unique interactions of the predicted VPS33B–VPS16B complex with SNAREs and vesicle membranes. *A*, in our predicted VPS33B–VPS16B complex structure, VPS33B proteins located at opposing ends are potentially capable of independently templating sets of fusogenic SNAREs (syntaxins, Qb, Qc, and R SNAREs), possibly allowing a single complex to template two sets of SNAREs at a site of membrane fusion. *B*, the predicted VPS33B–VPS16B complex may also be able to template SNAREpin formation at multiple sites where membranes are in close proximity, with each copy of VPS33B participating in an independent fusion event. SNARE, soluble *N*-ethylmaleimide-sensitive factor attachment protein receptor; VPS, vacuolar protein sorting protein.

(50 mM Tris, 150 mM NaCl, 1 mM EGTA, 1% Triton X-100, pH 7.4) with Roche cOmplete protease inhibitor cocktail (Sigma; catalog no.: CO-RO). After 5 min of lysis on ice, lysate was cleared by centrifugation at 16,100*g* at 4 °C for 20 min. About 20 μl of preconjugated M2 mouse-anti-FLAG agarose bead slurry (Sigma; catalog no.: A2220) or mouse immunoglobulin G agarose bead slurry were washed twice with lysis buffer before 700 μl of lysate was introduced. Beads were mixed with an end-over-end mixer for 1 h, then washed 5× with wash buffer with 0.1% Triton X-100, and once with Tris-buffered saline. FLAG beads were eluted using 50 μl 133 μg/ml 3xFLAG peptide in Tris-buffered saline on ice for 20 min. Mouse immunoglobulin G beads were eluted by adding 50 μl 1× SDS-PAGE sample buffer and heating at 95 °C for 5 min.

BN-PAGE

Precast Invitrogen NativePAGE 4 to 16% Bis–Tris Protein Gels (Thermo Fisher; catalog no.: BN1002BOX) in an XCell SureLock Mini gel tank (Thermo Fisher; catalog no.: EI0001) were utilized. Sample buffer, running, and transfer buffers were prepared according to the manufacturer's specifications. Gels were run at room temperature at constant 150 V for 3 h.

DAMI cell cultures

DAMI cells were grown to confluence in Iscove's media with 5% horse serum, in a 37 °C incubator with 5% CO_2 injection. For BN-PAGE, cells were pelleted at 400*g* for 3 min and lysed in lysis buffer (50 mM Tris, 150 mM NaCl, 1 mM EGTA, 0.5% Triton X-100, pH 7.4) for 1 h on ice. Lysate was cleared at 214,000*g* for 1 h at 4 °C, and the supernatant was dialyzed in 1 l 1× native sample buffer overnight at 4 °C.

Silver staining of polyacrylamide gels

SDS-PAGE or BN-PAGE gels that had been fixed (40% methanol, 10% acetic acid, 50% Milli-Q water v/v/v) for at least 15 min were equilibrated for 1 h in 50 ml Milli-Q water. The gels were rinsed once with Milli-Q water, reduced with sodium thiosulfate (20 mg in 100 ml Milli-Q water), and then rinsed twice with Milli-Q water for 30 s per rinse. Gels were stained in a clean glass container with 100 ml staining solution (100 mg silver nitrate in 100 ml Milli-Q water) for 25 to 30 min. Gels were rinsed twice with a small amount of developing solution (3 g sodium carbonate and 1 grain or approximately 1 mg of sodium thiosulfate in 100 ml Milli-Q water, supplemented with 140 μl 37% formaldehyde immediately before use) and developed in the remaining solution until satisfactorily stained, usually 30 s to 1 min. Development was stopped by replacing the developing solution with 1% v/v glacial acetic acid in Milli-Q water and allowing the gel to equilibrate for 20 min. All solutions are prepared fresh as needed.

Constructs and cloning

E. coli DH5α was used for all cloning and plasmid amplification. High-fidelity Pfu Ultra II DNA polymerase (VWR: CAST600672) was used for PCR amplification of inserts and site-directed mutagenesis.

We utilized a vector containing a bidirectional promoter formed from the fusion of the glyceraldehyde-3-phosphate dehydrogenase promoter with a shortened alcohol dehydrogenase (ADH1) promoter allowing constitutive expression of VPS33B and VPS16B-3xFLAG for in *S. cerevisiae* (44). pBEVY-T empty vector was a gift from Charles Miller (Addgene plasmid #51232; http://n2t.net/addgene:51232; Research

Resource Identifier: Addgene_51232). pCMV-Myc VPS33B was used as a template for PCR of untagged VPS33B. p3xFLAG-CMV-14 VPS16B was used as a template for VPS16B with C-terminal FLAG tag. VPS33B forward primer is S1V33FB4: CTAAGGGATCCATGGCTTTTCCCCATCGG CCG; VPS33B reverse primer is V33RBamHI: CTAA GGGATCCTCAGGCTTTCACCTCACTCATGGC; VPS16B-3xFLAG forward primer is S2V16FEcoRI: CTAAGGAATT CATGAATCGGACAAAGGGTGATGAGG; VPS16B-3xFLAG reverse primer is S2V16RE3: CTAAGGAATTCCTACTTGT CATCGTCATCCTTG. VPS33B was ligated into empty pBEVY-T using BamHI restriction site. VPS16B-3xFLAG was ligated into pBEVY-T containing VPS33B using EcoRI restriction site.

Site-directed mutagenesis primers for VPS33B are V33BL30P forward: AGCTCATCTATCTGCCGGAGCAG CTTC; V33BL30P reverse: GAAGCTGCTCCGGCAGATA GATGAGCT; V33BS243F forward: AGCACTTTGCTTCCA AGTGGTTTA; V33BS243FRev: TAAACCACTTGGAAGCA AAGTGCT; V33BH344D forward: CCTGCTGAGTCTCGA TATTGGGGCCTG; V33BH344D reverse: CAGGCCCCAA TATCGAGACTCAGCAGG.

VPS16B N-terminal truncation was generated by PCR using a new forward primer paired with the S2V16RE3 primer used to generate the pBEVY-T constructs with full-length VPS33B and VPS16B-3xFLAG. The PCR product was inserted into pBEVY-T already containing VPS33B using the EcoRI restriction site. Forward primer for generating the VPS16B truncation is V16T142FE: AAACAGAATTCATGAGACC CAAAGGGGAGTATAGG.

To generate pBEVY-T containing VPS33B and VPS16B(143–316)-3xFLAG, the VPS16B N-terminal truncation plasmid described previously was used as a template to produce a linear version of the plasmid with a SpeI restriction site downstream of amino acid 315 of VPS16B and one upstream of the 3xFLAG tag. The primers used are TV16BSpeIFDown: AATAACTAGTGACTACAAAGACCAT GACGGTG and TV16B315SpeIUp: AATAACTAGTCT GTCCTGCTGATTCTAGATGG. This PCR product was digested with SpeI and ligated to generate a circular plasmid.

The HA tag was added to the N terminus of VPS16B-3xFLAG within the pBEVY-T plasmid using the forward primer HA16F: CCGAGCTCGAATTCATG TACCCATAC GATGTTCCAGATTACGCT AATCGGACAAAGGGTG and the reverse primer HA16R: CACCCTTTGTCCGAT TAGCGTAATCTGGAACATCGTATGGGTA-CATGAATTCGAGCTCGG. The resulting pBEVY-T HA-VPS16B-3xFLAG plasmid was digested with SbfI. pCMV-HA VPS33B was used as a template for PCR of HA-tagged VPS33B flanked by SbfI restriction sites. This PCR product was digested with SbfI and ligated into pBEVY-T HA-VPS16B-3xFLAG. The HA-VPS33B forward primer is HA33FSbfI: AATACCTGCAGGATGTACCCATACGATGTTCCAGAT; the HA-VPS33B reverse primer is V33RSbfI: AATACCTG CAGGTCAGGCTTTCACCTCACTCATG.

To generated pBEVY-T containing HA-VPS33B and HA-tagged VPS16B(143–316)-3xFLAG, the pBEVY-T HA-VPS33B/HA-VPS16B-3xFLAG plasmid described previously was used as a template to generate a linear version of the plasmid with a SpeI restriction site in place of VPS16B. The primers are TV16BSpeIFDown: AATAACTAGTGACTA CAAAGACCATGACGGTG and THASpeIUp: AATAACT AGTAGCGTAATCTGGAACATCGT. This PCR product was digested with SpeI to generate a circular plasmid containing HA-SpeI-3xFLAG in place of HA-VPS16B-3xFLAG. VPS16B(143–316) fragment flanked by SpeI restriction sites was amplified by PCR and ligated into this vector. Primers used to amplify VPS16B(143–316) are V16D1-142FSpeI: AATAACTAGTAGACCCAAAGGGGAGTATAGG and TV16B315SpeIUp: AATAACTAGTCTGTCCTGCTGATTC TAGATGG.

C-terminal fusion of biotinylation signal on VPS33B was generated by overlapping PCR. VPS33B fragment was generated using the primers V33FSbfI: AATACCTGCAGGATGG CTTTTCCCCATCGGCC and V33BioOLr: CTCTCCGGCC TTACCGGCGGCTTTCACCTCACTCATG. Biotinylation signal was generated using the primers V33BioOLf: CAT GAGTGAGGTGAAAGCCGCCGGTAAGGCCGGAGAG and BioRSbfI: AATACCTGCAGGTCAGCCGATCTTGATGAGAC. Fragments were mixed and amplified in a PCR without primers for five cycles before V33FSbfI and BioRSbfI were added and PCR allowed to run to completion. The overlap product was digested with SbfI and ligated into pBEVY-T containing VPS16B-3xFLAG inserted at the EcoRI site.

Yeast transformation protocol

Lithium acetate/ssDNA transformation protocol was adapted from Gietz and Schiestl (69). Briefly, 50 ml yeast extract–peptone–dextrose (YPD) cultures are seeded from an overnight growth and grown at 30 °C with 210 rpm orbital agitation for 4 h or until an absorbance between 0.4 and 0.8 is reached at OD_{600} nm. Cells are pelleted and washed once with ultrapure water. Cells are resuspended in 2.5 ml LiAc/TE. About 100 ng of plasmid DNA is mixed with 100 μg of single-stranded DNA from salmon testis (Sigma; catalog no.: D7656). About 100 μl of resuspended cells are added to the plasmid–ssDNA mix, and 600 μl of LiAc/TE/PEG3350 are added. Cells are incubated at 30 °C with 210 rpm orbital agitation for 30 min. After incubation, 70 μl dimethyl sulfoxide is added, and cells are immediately heat-shocked for 10 to 15 min at 42 °C. Cells are allowed to recover for 2 min on ice and then pelleted by spinning briefly at >10,000*g* using a benchtop centrifuge. Pellets are resuspended in 500 μl YPD and allowed to recover overnight at room temperature without agitation. The next day, 150 μl of resuspended cells are plated on tryptophan dropout (Trp D.O.) agar plates and allowed to grow for 3 days at 30 °C. Plates were stored at 4 °C for up to 2 months.

Protein purification from yeast

BJ2168 yeast containing the selected pBEVY-T plasmid growing on Trp D.O. agar media was used to seed 5 ml Trp D.O. liquid culture for overnight growth at 30 °C. About 24 h later, the liquid culture was used to seed a 60 ml Trp D.O.

culture. After 24 h, this culture was used to seed five 1.4 l YPD cultures in 2800 ml baffle-less Fernbach flasks. The final growth was completed in a 30 °C incubator for 18 h with 210 rpm orbital agitation. Cells were pelleted using a JLA 9.1000 rotor for 15 min at 3000*g* and washed once with Milli-Q water. Each growth yielded 90 to 100 g washed cell pellet. Yeast was resuspended in 50 ml lysis buffer (20 mM Tris [pH 7.6], 200 mM NaCl, 10% sucrose, and 5 mM EDTA) with protease inhibitor (0.033 g 6-aminocaproic acid, 0.052 g 4-aminobenzamidine-2HCl, and 100 µl 2% PMSF in isopropanol), and lysed using a French Press at 1000 psi. Lysate was cleared by ultracentrifugation at 50,000*g* for 1 h at 4 °C using a Beckman SW28 rotor, and supernatant was filtered using a 0.45 µm syringe filter. Equal portions of cleared lysate were split between two 500 µl drip columns of m2 mouse anti FLAG-conjugated agarose beads (Sigma; catalog no.: A2220). After lysate has flowed through, beads were washed first with 10 ml high salt wash buffer (20 mM Tris, 400 mM NaCl, pH 7.6) and then with 10 ml low salt wash buffer (20 mM Tris, 200 mM NaCl, pH 7.6) without disturbing the packed bed. Aliquots of 3xFLAG peptide were diluted to a final concentration of 133 µg/ml using the low salt buffer. Each FLAG affinity column was incubated three times with 500 µl diluted FLAG peptide, for 15 min per incubation, followed by one incubation with 500 µl low salt buffer.

Ion exchange chromatography

For ion exchange chromatography, 1 ml GE HiTrap Q-HP anion exchange columns (VWR; catalog no.: CA95055-866L) and a GE AKTA Pure FPLC system were used. Purification was carried out in a 4 °C cold cabinet. The column was first equilibrated with at least five column volumes of low salt buffer (20 mM Tris, 200 mM NaCl, pH 7.6), and elutions 2, 3, and 4 from FLAG affinity column were then injected using a 5 ml injection loop prefilled with low salt buffer. Protein was eluted using a 200 to 450 mM NaCl gradient with 20 mM Tris (pH 7.6) over 15 1 ml fractions, at a flow rate of 1 ml/min. Samples were concentrated and exchanged into 20 mM Hepes buffer (pH 8.0) with 500 mM NaCl using Amicon mini concentrators with 100 kDa MW cutoff (Sigma; catalog no.: UFC510024).

Avidin labeling of VPS33B-biotin

The biotinylation signal was added to C terminus of VPS33B by overlapping PCR as described previously. The biotinylation signal consists of amino acids 49 to 123 of *Propionibacterium shermanii* transcarboxylase (methylmalonyl-CoA carboxyltransferase 1.3S subunit; UniProt: P02904), corresponding to its biotinyl-binding domain. The amino acid sequence of this biotinylation signal is AGKAGEGEIPAPLAGTVSKILVKE GDTVKAGQTVLVLEAM**K**METEINAPTDGKVEKVLVKERD AVQGGQGLIKIG

When expressed in yeast, this sequence is recognized by the endogenous biotinylation machinery and lysine 41 (bolded and underlined in the aforementioned sequence) becomes biotinylated.

The DNA sequence used to encode this biotinylation signal is GCCGGTAAGGCCGGAGAGGGCGAGATTCCCGCTCC GCTGGCCGGCACCGTCTCCAAGATCCTCGTGAAGGAG GGTGACACGGTCAAGGCTGGTCAGACCGTGCTCGTTC TCGAGGCCATGAAGATGGAGACCGAGATCAACGCTC CCACCGACGGCAAGGTCGAGAAGGTCCTTGTCAAGGA GCGTGACGCCGTGCAGGGCGGTCAGGGTCTCATCAA GATCGGCTGA.

Egg white avidin stock (BioShop; catalog no.: AVD407) was reconstituted in Milli-Q water at a concentration of 20 mg/ml and stored frozen at −20 °C in 50 µl aliquots. For use, 25 µl of avidin stock was diluted with 1 ml 20 mM Hepes buffer (pH 8.0) with 200 mM NaCl to 0.5 mg/ml final concentration.

Biotinylated VPS33B in complex with VPS16B-3xFLAG was expressed in yeast and loaded onto FLAG-affinity column as described previously. After washing with low salt wash buffer, 1 ml diluted avidin was introduced to the column and allowed to flow through, labeling biotinylated VPS33B immobilized on FLAG-affinity column. Excess avidin was removed by washing with 20 mM Hepes/200 mM NaCl. Elution was performed as aforementioned, except with FLAG peptide diluted in 20 mM Hepes/200 mM NaCl instead of low salt buffer. For quality control, samples of biotinylated VPS33B with avidin were mixed with SDS-PAGE running buffer and either incubated at 95 °C for 5 min or stored at room temperature for the same time, and both samples were then resolved on SDS-PAGE gel. The absence of free VPS33B-Bio band in sample that was not heated indicates robust avidin labeling.

Mass spectrometry

Bands were excised from Coomassie-stained gels and collected in a 1.5 ml Eppendorf tube. After washing with 50 µl of 50 mM ammonium bicarbonate, remaining Coomassie was removed with 50 µl of 50% v/v acetonitrile/25 mM ammonium bicarbonate. The sample was reduced with 30 µl of 10 mM DTT in 50 mM ammonium bicarbonate for 30 min at 56 °C and then alkylated with 30 µl of 100 mM iodoacetamide for 15 min at room temperature. Excess water was then removed by washing the excised band with 50 µl of 50% acetonitrile/25 mM ammonium bicarbonate as aforementioned. In-gel digestion of protein sample was performed by covering the excised band with 50 µl of 13 ng/µl MS-grade trypsin (Thermo Fisher Scientific; catalog no.: 90057) in 50 mM ammonium bicarbonate and incubating overnight at 37 °C. Peptides were extracted from the gel by washing twice alternately with 5% formic acid and 100% acetonitrile and collecting the supernatant (after 10 min incubation). Peptides were dried in a SpeedVac and reconstituted in 5 µl of 0.1% v/v formic acid in Milli-Q water. C18 Ziptip cleanup and MALDI-MS were performed by the SPARC BioCentre, The Hospital for Sick Children, Toronto, Canada.

SAXS

VPS33B/VPS16B-3xFLAG in solution at 0.92 mg/ml with 20 mM Tris (pH 7.6) and 320 mM NaCl was used for SAXS. Fresh buffer showed no significant scattering. SAXS

data were collected in 24 × 5 min accumulations. SAXS was performed in 1D line collimation mode on an Anton Paar SAXSpace System with SAXSdrive, version 2.02.250.13277. SAXStreat, version 1.06.003.8398 was used to export data in a suitable format for analysis with SAXSquant, version 4.1.1.8319.

Circular dichroism

Circular dichroism was performed using a Jasco J-1500 circular dichroism spectrophotometer. Pure protein sample at 0.1 mg/ml in 500 mM NaCl and 20 mM phosphate buffer (pH 8.0) was loaded in a Hellma High Precision quartz cell with path length of 1 mm. The buffer had no significant absorbance in the 190 to 280 nm range. Data were collected at 20 nm/min from 280 to 190 nm.

SEC–MALS

SEC–MALS was performed by the Biophysical Core Facility at the Peter Gilgan Centre for Research and Learning. A 1260 Infinity II bio-inert HPLC with AdvanceBio SEC300A 2.7 μm 4.6 × 300 mm column was used. SEC–MALS was performed at 4 °C with 20 mM Hepes (pH 8.0) with 500 mM NaCl at 0.2 ml/min flow rate. Data were collected using a Mini-DAWNTREOS MALS, Quasi-Elastic Light Scattering, and OptiLabT-rEXRefractive Index detection instrument (Wyatt Technology), along with UV_{280} chromatogram. Samples were centrifuged at >20,000*g* for 10 to 15 min at 4 °C to remove any aggregates or insoluble particulates. About 20 to 25 μl of sample at 0.25 to 0.5 mg/ml were injected. Fractions were collected every 30 s (100 μl per fraction). Chromatogram data were analyzed using ASTRA software (Wyatt) with a UV_{280} 0.1% of 0.903 ml/(mg cm), dn/dc of 0.185, and refractive index 0 to the supplied buffer to determine the MWs of the protein chromatographic peaks.

Quantitative immunoblotting

Complexes containing N-terminal HA-tagged VPS33B and N-terminal HA-tagged VPS16B-3xFLAG were purified from yeast using FLAG affinity followed by anion exchange as described. Pure protein concentrations were measured by A_{280} nm using a NanoDrop 1000 spectrophotometer. Serial dilutions were loaded on a 10% SDS-PAGE gel, with 0.04 μg as the maximum total protein in a lane followed by a dilution series with 0.01, 0.0025, 0.000625, and 0.0003125 μg. Proteins were transferred to nitrocellulose membrane by wet transfer, for 1:30 h at 100 V. The membrane was blocked with 4% w/v bovine serum albumin in Tris-buffered saline with Tween-20. Monoclonal mouse anti HA was diluted 1:1000 in blocking buffer. Secondary antibody was Alexa Fluor 488–conjugated donkey antimouse diluted 1:5000 in blocking buffer. After 1 h incubation with secondary antibody in the dark, the membrane was washed with PBS before imaging using a BioRad Chem-iDoc XRS+. Analysis was performed using Image Lab software, version 6.1 with manual lane assignment and automatic band detection at the low-sensitivity band detection setting.

Complex crosslinking

Affinity-purified VPS33B–VPS16B-3xFLAG (0.3–0.5 mg/ml) in 20 mM Hepes (pH 8.0) and 500 mM NaCl was crosslinked with 0.01% v/v glutaraldehyde at 42 °C for 5 min. Glutaraldehyde was quenched by adding 1/20 volume of 1 M Tris (pH 7.8). Samples were either used immediately for EM grid preparation or stored at 4 °C for up to 24 h before use. For avidin-labeled biotinylated VPS33B, crosslinking was performed in 20 mM Hepes (pH 8.0) and 200 mM NaCl.

Negative-staining EM

Carbon-coated copper–rhodium grids were prepared according to Booth *et al.* (70). Protein complexes were diluted to between 0.01 and 0.05 mg/ml in 20 mM Hepes (pH 8.0) with 500 mM NaCl, except for avidin-labeled biotinylated VPS33B, which was diluted in 20 mM Hepes (pH 8.0) with 200 mM NaCl. Grids were glow discharged for 15 s, then 4 μl of sample was pipetted onto the grid and allowed to bind for 2 min at room temperature. Excess sample was removed by edge blotting onto Whatman filter paper (Sigma; catalog no.: Z240079). Grids were washed three times in 50 μl drops of Milli-Q water and stained with 2% uranyl formate in Milli-Q water. Excess uranyl formate was removed by edge blotting, and grids were allowed to air dry. Micrographs were collected on an FEI Tecnai F20 TEM at 25,000× magnification using a Gatan Orius SC1000 CCD, with a pixel size of 2.61 Å. Relion 2.1 was used for manual particle picking and 2D classification. AlphaFold was used for *ab initio* 3D reconstruction.

Antibodies

Antibody	Company, catalog number	Dilution for Western blotting
Rabbit anti-VPS33B	Abcam, Ab153844	1/1000
Rabbit anti-C14orf133/ VIPAR (VPS16B)	Abcam/ThermoFisher, Ab125084/A303-526A	1/1000
Rabbit anti-HA	Bethyl, A190-208A	1/1000
Monoclonal M2 anti-FLAG	Sigma–Aldrich, F3165	1/5000
Rabbit anti-FLAG	Sigma–Aldrich, F7425	1/1000
Rabbit anti-Myc	Sigma–Aldrich, C3956	1/1000
Monoclonal anti-HA	Covance, MMS-101P	1/1000
AF488-donkey antimouse	ThermoFisher, A-21202	1/5000
Monoclonal anti-α-tubulin	Sigma–Aldrich, T 6074	1/5000

Data availability

All the data are contained within the article.

Supporting information—This article contains supporting information.

Author contributions—R. J. Y. L., Y. A-M., S. Z. C., M. D., D. U., C. H. C., H. H. Y. Y., R. S. Q. G., L. L., F. G. P., S. B., J. L. R., and W. H. A. K. investigation; S. B. and J. L. R. resources; R. J. Y. L. and W. H. A. K. writing–original draft; R. J. Y. L., Y. A-M., S. Z. C., M. D., D. U., C. H. C., H. H. Y. Y., R. S. Q. G., L. L., and F. G. P. writing–review & editing; S. B., J. L. R., and W. H. A. K. supervision.

Funding and additional information—R. J. Y. L. was supported by a Natural Sciences and Engineering Research Council of Canada Graduate Scholarship Master's program and a Natural Sciences and Engineering Research Council of Canada Postgraduate Scholarship Doctoral program. R. J. Y. L. and R. S. Q. G. were supported by the RESTRACOMP fellowship from the Research Institute of the Hospital for Sick Children, Toronto, Canada. W. H. A. K. is supported by an operating grant from the Canadian Institutes of Health Research (grant no.: PJT156095).

Conflict of interest—The authors declare that they have no conflicts of interest with the contents of this article.

Abbreviations—The abbreviations used are: ARC, arthrogryposis, renal dysfunction, and cholestasis; BN-PAGE, blue native polyacrylamide gel electrophoresis; co-IP, coimmunoprecipitation; CORVET, class C core vacuole/endosome tethering; DAMI, megakaryoblastic DAMI cell line; HA, hemagglutinin; HEK293, human embryonic kidney 293 cell line; HOPS, homotypic fusion and vacuole protein sorting; MW, molecular weight; SAXS, small-angle X-ray scattering; SEC–MALS, size-exclusion chromatography–multiangle light scattering; SM, Sec1–Munc18; SNARE, soluble N-ethylmaleimide sensitive factor attachment protein receptor; Trp D.O., tryptophan dropout media; VPS, vacuolar protein sorting protein; YPD, yeast extract–peptone–dextrose.

References

1. Cullinane, A. R., Straatman-Iwanowska, A., Zaucker, A., Wakabayashi, Y., Bruce, C. K., Luo, G., *et al.* (2010) Mutations in VIPAR cause an arthrogryposis, renal dysfunction and cholestasis syndrome phenotype with defects in epithelial polarization. *Nat. Genet.* **42**, 303–312
2. Gissen, P., Johnson, C. A., Morgan, N. V., Stapelbroek, J. M., Forshew, T., Cooper, W. N., *et al.* (2004) Mutations in VPS33B, encoding a regulator of SNARE-dependent membrane fusion, cause arthrogryposis-renal dysfunction-cholestasis (ARC) syndrome. *Nat. Genet.* **36**, 400–404
3. Chen, C. H., Lo, R. W., Urban, D., Pluthero, F. G., and Kahr, W. H. (2017) alpha-granule biogenesis: from disease to discovery. *Platelets* **28**, 147–154
4. Lo, B., Li, L., Gissen, P., Christensen, H., McKiernan, P. J., Ye, C., *et al.* (2005) Requirement of VPS33B, a member of the Sec1/Munc18 protein family, in megakaryocyte and platelet α-granule biogenesis. *Blood* **106**, 4159–4166
5. Urban, D., Li, L., Christensen, H., Pluthero, F. G., Chen, S. Z., Puhacz, M., *et al.* (2012) The VPS33B-binding protein VPS16B is required in megakaryocyte and platelet alpha-granule biogenesis. *Blood* **120**, 5032–5040
6. Akbar, M. A., Mandraju, R., Tracy, C., Hu, W., Pasare, C., and Kramer, H. (2016) ARC syndrome-linked Vps33B protein is required for inflammatory endosomal maturation and signal termination. *Immunity* **45**, 267–279
7. Akbar, M. A., Tracy, C., Kahr, W. H., and Kramer, H. (2011) The full-of-bacteria gene is required for phagosome maturation during immune defense in Drosophila. *J. Cell Biol.* **192**, 383–390
8. Banushi, B., Forneris, F., Straatman-Iwanowska, A., Strange, A., Lyne, A. M., Rogerson, C., *et al.* (2016) Regulation of post-Golgi LH3 trafficking is essential for collagen homeostasis. *Nat. Commun.* **7**, 12111
9. Bem, D., Smith, H., Banushi, B., Burden, J. J., White, I. J., Hanley, J., *et al.* (2015) VPS33B regulates protein sorting into and maturation of alpha-granule progenitor organelles in mouse megakaryocytes. *Blood* **126**, 133–143
10. Rogerson, C., and Gissen, P. (2018) VPS33B and VIPAR are essential for epidermal lamellar body biogenesis and function. *Biochim. Biophys. Acta Mol. Basis Dis.* **1864**, 1609–1621
11. Dai, J., Lu, Y., Wang, C., Chen, X., Fan, X., Gu, H., *et al.* (2016) Vps33b regulates Vwf-positive vesicular trafficking in megakaryocytes. *J. Pathol.* **240**, 108–119
12. Galmes, R., ten Brink, C., Oorschot, V., Veenendaal, T., Jonker, C., van der Sluijs, P., *et al.* (2015) Vps33B is required for delivery of endocytosed cargo to lysosomes. *Traffic* **16**, 1288–1305
13. Bonifacino, J. S., and Glick, B. S. (2004) The mechanisms of vesicle budding and fusion. *Cell* **116**, 153–166
14. Liu, Y., Wan, C., Rathore, S. S., Stowell, M. H. B., Yu, H., and Shen, J. (2021) SNARE zippering is Suppressed by a conformational Constraint that is removed by v-SNARE Splitting. *Cell Rep.* **34**, 108611
15. Zhang, Y., and Hughson, F. M. (2021) Chaperoning SNARE folding and assembly. *Annu. Rev. Biochem.* **90**, 581–603
16. Brunger, A. T. (2005) Structure and function of SNARE and SNARE-interacting proteins. *Q. Rev. Biophys.* **38**, 1–47
17. Jahn, R., and Sudhof, T. C. (1999) Membrane fusion and exocytosis. *Annu. Rev. Biochem.* **68**, 863–911
18. Wickner, W. (2010) Membrane fusion: five lipids, four SNAREs, three chaperones, two nucleotides, and a Rab, all dancing in a ring on yeast vacuoles. *Annu. Rev. Cell Dev. Biol.* **26**, 115–136
19. Baker, R. W., and Hughson, F. M. (2016) Chaperoning SNARE assembly and disassembly. *Nat. Rev. Mol. Cell Biol.* **17**, 465–479
20. Hong, W., and Lev, S. (2014) Tethering the assembly of SNARE complexes. *Trends Cell Biol.* **24**, 35–43
21. Seals, D. F., Eitzen, G., Margolis, N., Wickner, W. T., and Price, A. (2000) A Ypt/Rab effector complex containing the Sec1 homolog Vps33p is required for homotypic vacuole fusion. *Proc. Natl. Acad. Sci. U. S. A.* **97**, 9402–9407
22. Peplowska, K., Markgraf, D. F., Ostrowicz, C. W., Bange, G., and Ungermann, C. (2007) The CORVET tethering complex interacts with the yeast Rab5 homolog Vps21 and is involved in endo-lysosomal biogenesis. *Dev. Cell* **12**, 739–750
23. Sato, T. K., Rehling, P., Peterson, M. R., and Emr, S. D. (2000) Class C Vps protein complex regulates vacuolar SNARE pairing and is required for vesicle docking/fusion. *Mol. Cell* **6**, 661–671
24. Baker, R. W., Jeffrey, P. D., Zick, M., Phillips, B. P., Wickner, W. T., and Hughson, F. M. (2015) A direct role for the Sec1/Munc18-family protein Vps33 as a template for SNARE assembly. *Science* **349**, 1111–1114
25. Shvarev, D., Schoppe, J., Konig, C., Perz, A., Fullbrunn, N., Kiontke, S., *et al.* (2022) Structure of the HOPS tethering complex, a lysosomal membrane fusion machinery. *Elife* **11**, e80901
26. Balderhaar, H. J., and Ungermann, C. (2013) CORVET and HOPS tethering complexes - coordinators of endosome and lysosome fusion. *J. Cell Sci.* **126**, 1307–1316
27. Zhu, G. D., Salazar, G., Zlatic, S. A., Fiza, B., Doucette, M. M., Heilman, C. J., *et al.* (2009) SPE-39 family proteins interact with the HOPS complex and function in lysosomal delivery. *Mol. Biol. Cell* **20**, 1223–1240
28. Zlatic, S. A., Tornieri, K., L'Hernault, S. W., and Faundez, V. (2011) Clathrin-dependent mechanisms modulate the subcellular distribution of class C Vps/HOPS tether subunits in polarized and nonpolarized cells. *Mol. Biol. Cell* **22**, 1699–1715
29. Graham, S. C., Wartosch, L., Gray, S. R., Scourfield, E. J., Deane, J. E., Luzio, J. P., *et al.* (2013) Structural basis of Vps33A recruitment to the human HOPS complex by Vps16. *Proc. Natl. Acad. Sci. U. S. A.* **110**, 13345–13350
30. van der Kant, R., Jonker, C. T., Wijdeven, R. H., Bakker, J., Janssen, L., Klumperman, J., *et al.* (2015) Characterization of the mammalian CORVET and HOPS complexes and their modular restructuring for endosome specificity. *J. Biol. Chem.* **290**, 30280–30290
31. Wartosch, L., Gunesdogan, U., Graham, S. C., and Luzio, J. P. (2015) Recruitment of VPS33A to HOPS by VPS16 is required for lysosome fusion with endosomes and autophagosomes. *Traffic* **16**, 727–742
32. Gu, H., Chen, C., Hao, X., Wang, C., Zhang, X., Li, Z., *et al.* (2016) Sorting protein VPS33B regulates exosomal autocrine signaling to mediate hematopoiesis and leukemogenesis. *J. Clin. Invest.* **126**, 4537–4553
33. Perini, E. D., Schaefer, R., Stoter, M., Kalaidzidis, Y., and Zerial, M. (2014) Mammalian CORVET is required for fusion and conversion of distinct early endosome subpopulations. *Traffic* **15**, 1366–1389
34. Pulipparacharuvil, S., Akbar, M. A., Ray, S., Sevrioukov, E. A., Haberman, A. S., Rohrer, J., *et al.* (2005) Drosophila Vps16A is required for

trafficking to lysosomes and biogenesis of pigment granules. *J. Cell Sci.* **118**, 3663–3673
35. Akbar, M. A., Ray, S., and Kramer, H. (2009) The SM protein Car/Vps33A regulates SNARE-mediated trafficking to lysosomes and lysosome-related organelles. *Mol. Biol. Cell* **20**, 1705–1714
36. Matthews, R. P., Plumb-Rudewiez, N., Lorent, K., Gissen, P., Johnson, C. A., Lemaigre, F., *et al.* (2005) Zebrafish vps33b, an ortholog of the gene responsible for human arthrogryposis-renal dysfunction-cholestasis syndrome, regulates biliary development downstream of the onecut transcription factor hnf6. *Development* **132**, 5295–5306
37. Suzuki, T., Oiso, N., Gautam, R., Novak, E. K., Panthier, J. J., Suprabha, P. G., *et al.* (2003) The mouse organellar biogenesis mutant buff results from a mutation in Vps33a, a homologue of yeast vps33 and drosophila carnation. *Proc. Natl. Acad. Sci. U. S. A.* **100**, 1146–1150
38. Rogerson, C., and Gissen, P. (2016) The CHEVI tethering complex: facilitating special deliveries. *J. Pathol.* **240**, 249–252
39. Spang, A. (2016) Membrane tethering complexes in the endosomal system. *Front. Cell Dev. Biol.* **4**, 35
40. Hunter, M. R., Hesketh, G. G., Benedyk, T. H., Gingras, A. C., and Graham, S. C. (2018) Proteomic and biochemical comparison of the cellular interaction partners of human VPS33A and VPS33B. *J. Mol. Biol.* **430**, 2153–2163
41. Ambrosio, A. L., and Di Pietro, S. M. (2019) Mechanism of platelet alpha-granule biogenesis: study of cargo transport and the VPS33B-VPS16B complex in a model system. *Blood Adv.* **3**, 2617–2626
42. Kahr, W. H., Pluthero, F. G., Elkadri, A., Warner, N., Drobac, M., Chen, C. H., *et al.* (2017) Loss of the Arp2/3 complex component ARPC1B causes platelet abnormalities and predisposes to inflammatory disease. *Nat. Commun.* **8**, 14816
43. Wittig, I., Braun, H. P., and Schagger, H. (2006) Blue native PAGE. *Nat. Protoc.* **1**, 418–428
44. Miller, C. A., 3rd, Martinat, M. A., and Hyman, L. E. (1998) Assessment of aryl hydrocarbon receptor complex interactions using pBEVY plasmids: expressionvectors with bi-directional promoters for use in Saccharomyces cerevisiae. *Nucleic Acids Res.* **26**, 3577–3583
45. Greenfield, N. J. (2006) Using circular dichroism spectra to estimate protein secondary structure. *Nat. Protoc.* **1**, 2876–2890
46. Brocker, C., Kuhlee, A., Gatsogiannis, C., Balderhaar, H. J., Honscher, C., Engelbrecht-Vandre, S., *et al.* (2012) Molecular architecture of the multisubunit homotypic fusion and vacuole protein sorting (HOPS) tethering complex. *Proc. Natl. Acad. Sci. U. S. A.* **109**, 1991–1996
47. Smith, H., Galmes, R., Gogolina, E., Straatman-Iwanowska, A., Reay, K., Banushi, B., *et al.* (2012) Associations among genotype, clinical phenotype, and intracellular localization of trafficking proteins in ARC syndrome. *Hum. Mutat.* **33**, 1656–1664
48. Penon-Portmann, M., Westbury, S. K., Li, L., Pluthero, F. G., Liu, R. J. Y., Yao, H. H. Y., *et al.* (2022) Platelet VPS16B is dependent on VPS33B expression, as determined in two siblings with arthrogryposis, renal dysfunction, and cholestasis syndrome. *J. Thromb. Haemost.* **20**, 1712–1719
49. Tornieri, K., Zlatic, S. A., Mullin, A. P., Werner, E., Harrison, R., L'Hernault S, W., *et al.* (2013) Vps33b pathogenic mutations preferentially affect VIPAS39/SPE-39-positive endosomes. *Hum. Mol. Genet.* **22**, 5215–5228
50. Jumper, J., Evans, R., Pritzel, A., Green, T., Figurnov, M., Ronneberger, O., *et al.* (2021) Highly accurate protein structure prediction with AlphaFold. *Nature* **596**, 583–589
51. Tunyasuvunakool, K., Adler, J., Wu, Z., Green, T., Zielinski, M., Zidek, A., *et al.* (2021) Highly accurate protein structure prediction for the human proteome. *Nature* **596**, 590–596
52. AlQuraishi, M. (2021) Protein-structure prediction revolutionized. *Nature* **596**, 487–488
53. Rubinstein, J. L., Dickson, V. K., Runswick, M. J., and Walker, J. E. (2005) ATP synthase from saccharomyces cerevisiae: location of subunit h in the peripheral stalk region. *J. Mol. Biol.* **345**, 513–520
54. Hosono, R., Hekimi, S., Kamiya, Y., Sassa, T., Murakami, S., Nishiwaki, K., *et al.* (1992) The unc-18 gene encodes a novel protein affecting the kinetics of acetylcholine metabolism in the nematode Caenorhabditis elegans. *J. Neurochem.* **58**, 1517–1525
55. Novick, P., Field, C., and Schekman, R. (1980) Identification of 23 complementation groups required for post-translational events in the yeast secretory pathway. *Cell* **21**, 205–215
56. Rizo, J., and Sudhof, T. C. (2012) The membrane fusion enigma: SNAREs, sec1/Munc18 proteins, and their accomplices–guilty as charged? *Annu. Rev. Cell Dev. Biol.* **28**, 279–308
57. Sudhof, T. C., and Rothman, J. E. (2009) Membrane fusion: grappling with SNARE and SM proteins. *Science* **323**, 474–477
58. Toonen, R. F., and Verhage, M. (2007) Munc18-1 in secretion: lonely munc joins SNARE team and takes control. *Trends Neurosci.* **30**, 564–572
59. Jiao, J., He, M., Port, S. A., Baker, R. W., Xu, Y., Qu, H., *et al.* (2018) Munc18-1 catalyzes neuronal SNARE assembly by templating SNARE association. *Elife* **7**, e41771
60. Ambrosio, A. L., Febvre, H. P., and Di Pietro, S. M. (2021) Syntaxin 12 and COMMD3 are new factors that function with VPS33B in the biogenesis of platelet alpha-granules. *Blood* **139**, 922–935
61. Saitsu, H., Kato, M., Mizuguchi, T., Hamada, K., Osaka, H., Tohyama, J., *et al.* (2008) De novo mutations in the gene encoding STXBP1 (MUNC18-1) cause early infantile epileptic encephalopathy. *Nat. Genet.* **40**, 782–788
62. Stepensky, P., Saada, A., Cowan, M., Tabib, A., Fischer, U., Berkun, Y., *et al.* (2013) The Thr224Asn mutation in the VPS45 gene is associated with the congenital neutropenia and primary myelofibrosis of infancy. *Blood* **121**, 5078–5087
63. Vilboux, T., Lev, A., Malicdan, M. C., Simon, A. J., Jarvinen, P., Racek, T., *et al.* (2013) A congenital neutrophil defect syndrome associated with mutations in VPS45. *N. Engl. J. Med.* **369**, 54–65
64. Korteweg, N., Maia, A. S., Thompson, B., Roubos, E. W., Burbach, J. P., and Verhage, M. (2005) The role of Munc18-1 in docking and exocytosis of peptide hormone vesicles in the anterior pituitary. *Biol. Cell* **97**, 445–455
65. Gutierrez, B. A., Chavez, M. A., Rodarte, A. I., Ramos, M. A., Dominguez, A., Petrova, Y., *et al.* (2018) Munc18-2, but not Munc18-1 or Munc18-3, controls compound and single-vesicle-regulated exocytosis in mast cells. *J. Biol. Chem.* **293**, 7148–7159
66. Frey, L., Zietara, N., Lyszkiewicz, M., Marquardt, B., Mizoguchi, Y., Linder, M. I., *et al.* (2021) Mammalian VPS45 orchestrates trafficking through the endosomal system. *Blood* **137**, 1932–1944
67. Brandhorst, D., Zwilling, D., Rizzoli, S. O., Lippert, U., Lang, T., and Jahn, R. (2006) Homotypic fusion of early endosomes: SNAREs do not determine fusion specificity. *Proc. Natl. Acad. Sci. U. S. A.* **103**, 2701–2706
68. Solinger, J. A., Rashid, H. O., Prescianotto-Baschong, C., and Spang, A. (2020) FERARI is required for Rab11-dependent endocytic recycling. *Nat. Cell Biol.* **22**, 213–224
69. Gietz, R. D., and Schiestl, R. H. (2007) High-efficiency yeast transformation using the LiAc/SS carrier DNA/PEG method. *Nat. Protoc.* **2**, 31–34
70. Booth, D. S., Avila-Sakar, A., and Cheng, Y. (2011) Visualizing proteins and macromolecular complexes by negative stain EM: from grid preparation to image acquisition. *J Vis. Exp.* https://doi.org/10.3791/3227